Chapter 5

Synthesis, Characterization and Magnetic Properties of Cyano Bridged Heterometallic Mn(II)-Fe(II)/Fe(III) Aggregates

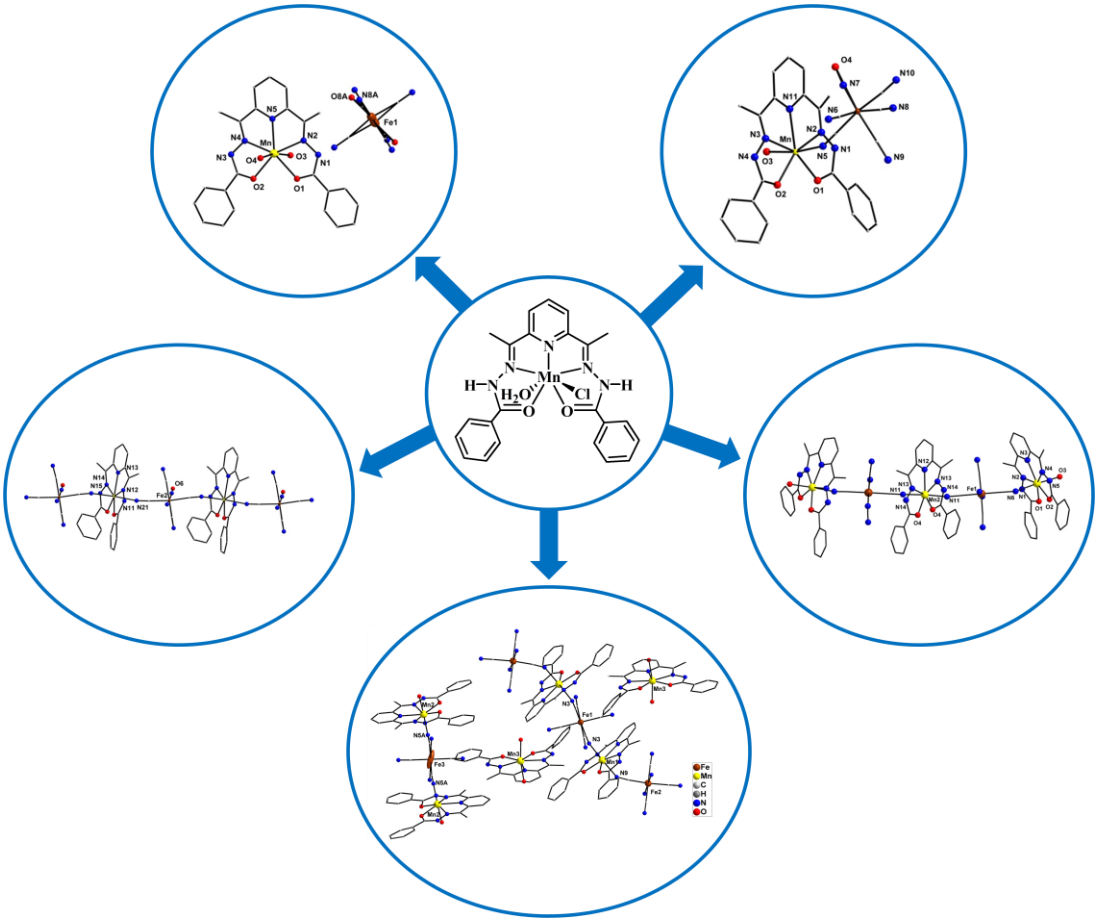

Abstract: The possibility to control the aggregation pattern of pentagonal bipyramidal Mn(II) complex formed by 2,6-diacetylpyridine bis(benzoylhydrazone) with sodium nitroprusside and potassium ferricyanide as metalloligands has been explored. Syntheses, characterization, structures and magnetic properties of five new heterometallic complexes have been reported.

5.1. Introduction

The discovery of high T_c molecule based magnetism in Prussian Blue analogues have led to an outburst of activities in cyano bridged architectures [1]. During the last two decades, cyano bridged assemblies exhibiting a fascinating assortment of intriguing characteristics e.g. room temperature magnetism [2], spin-crossover [3], single molecule magnetism [4-6], single chain magnetism [7-8], photomagnetism [9], etc. have been developed. These versatile features of cyano bridged aggregates can be primarily attributed to the short and effective magnetic superexchange mediated by bridging cyano groups. Further, due to the interplay of strong exchange interaction between the spin carriers, the magnetic and photomagnetic properties of cyano bridged assemblies are largely governed by their structural topology and nuclearity. Therefore, rational approaches to build discrete cyano-bridged polynuclear assemblies of predetermined structure has so far remained a highly desirable and fundamental goal in contemporary molecular magnetism [7-13]. Fortunately, the linear coordination mode of cyano ligand facilitates reasonable prediction of the structure of the resulting cyano bridged architectures. Moreover, the nature of magnetic superexchange between the spin carriers can also be controlled by careful choice of the precursors. In view of the above, bottom up assembling of suitable building blocks by using cyanometallate linkers have emerged as one of the most prolific approach to engineer cyano bridged species of desired topology and dimensionality [14-17].

Mononuclear complexes of rigid macrocyclic ligands with labile axial sites have emerged as highly preferred choice of building blocks for bottom up assembly of cyanometallate aggregates [18-21]. Substitution of the labile axial sites in such complexes by cyanometallate linkers have resulted in cyano bridged heteronuclear aggregates of varied topology, nuclearity and dimensionality. Further, the structure and dimensionality of these species can be efficiently modulated by using capping ligands either in the cyanometallate linker or in the macrocyclic complex [22-25]. Apart from the above, several other parameters *viz.* charge on the assembling units, solvent and ancillary ligands used also play crucial roles in determining the final structure of the resulting species.

The macrocyclic complex based building block approach to design cyano bridged heterometallic aggregates has been also extended for PBP complexes. It is pertinent to note here that many transition metal ions display large single ion anisotropy in PBP

geometry [26-27]. Therefore heterometallic aggregates assembled from magnetically anisotropic PBP transition metal building blocks and cyanometallates have emerged as prospective candidates for single molecule magnets. For example, due to the presence of inherent magnetic anisotropy in PBP complexes of Fe(II), Co(II) and Ni(II), the resulting cyano bridged heterometallic assemblies show SMM behaviour [27-34].

Reaction of PBP Mn(II) complexes with different cyanometallate precursors have so far resulted in discrete dinculear, trinuclear, pentanuclear aggregates in addition to 1D, 2D and 3D architectures [29, 35-45]. The planer pentadentate ligand, 2,6-diacetylpyridine bis(benzoyl hydrazone) (H_2L) allows isolation of several PBP transition metal complexes [44-45]. The axial sites of these complexes are usually occupied by labile groups. This facilitates rapid reaction with metallo-ligands e.g. cyanometallates. Moreover, the PBP geometry around the 3d metal center can be retained in the resulting heterometallic structures [33, 46].

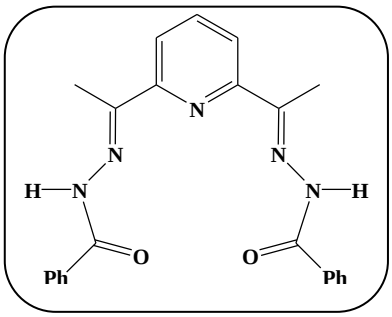

Chart 5.1. The ligand 2,6-diacetylpyridine bis(benzoyl hydrazone) (H_2L)

In the present study, we have investigated the possibility to control the self assembly process of seven coordinated Mn(II) complexes, $[Mn(H_2L)(H_2O)Cl]Cl$ formed by 2,6-diacetylpyridine bis(benzoyl hydrazone) with different cyanometallate based metalloligands. The precursor complex, $[Mn(H_2L)(H_2O)Cl]Cl$ has labile axial ligands and therefore expected to undergo spontaneous self-assembly with cyanometallate linkers. Further, the resulting heterometallic structures of such charge-mediated self-assembly processes are strongly dependent on the charge of the PBP precursor as well as cyanometallate linker. Therefore, the reaction of $[Mn(H_2L)(H_2O)Cl]Cl$ was studied with two different cyanometallate linker, $[Fe(CN)_5(NO)]^{2+}$ and $[Fe(CN)_6]^{3-}$. Dependence of subtle variations in the reaction conditions or reactants on the architecture of the resulting heteronuclear assemblages have been explored to gain better understanding of the self assembling process. Initial investigations were carried

out by mixing nitroprusside as the linker. Nitroprusside based assemblies are particularly interesting due to its intriguing photophysical properties [47-48]. But due to the diamagnetic character of nitroprusside ion, cooperative magnetic phenomena are not expected in the resulting heterometallic architectures. Therefore, we later switched to a paramagnetic cyanometallate precursor, $[Fe(CN)_6]^{3-}$ and investigated its reaction with $[Mn(H_2L)(H_2O)Cl]Cl$. Facile substitution of the axial coordination sites of $[Mn(H_2L)(H_2O)Cl]Cl$ by cyanometallate precursors leading to the formation of heterometallic cyano bridged Mn(II)-Fe(III) aggregates was observed. Thus, five new cyanobridged heterometallic Mn(II)-Fe(II)/Fe(III) assemblages, $[Mn(H_2L)(H_2O)_2][Fe(CN)_5(NO)].H_2O$ (**15**), $[\{Mn(H_2L)\}\{Fe(CN)_5(NO)\}]$ (**16**), $[\{Mn(H_2L)\}\{Fe(CN)_5(NO)\}\cdot(H_2O)_{0.75}]_n$(**17)**, **[**$\{Mn(H_2L)(H_2O)\}_2\{Mn(H_2L)\}\{Fe(CN)_6\}_2].9H_2O$ (**18**) and $[Mn(H_2L)(H_2O)_2]_2[\{Mn(H_2L)(H_2O)\}_2\{Fe(CN)_6\}][\{Mn(H_2L)\}_2\{Fe(CN)_6\}_3].13H_2O$(**19**) are prepared. The syntheses, characterization and magnetic properties of these compounds have been reported in this chapter.

5.2. Experimental Section

5.2.1. Materials and Methods

Starting materials were procured from commercial sources and used as received. Solvents were purified by conventional techniques and distilled prior to use. 2,6-diacetylpyridine bis(benzoyl hydrazone) and $[Mn(H_2L)Cl(H_2O)]Cl$ were prepared according to the reported literature procedure [45-46]. Elemental analyses were performed on a Perkin Elmer Model PR 2400 Series II Elemental Analyzer. Infrared spectra were recorded on a Nicolet Impact I-410 FT-IR spectrometer as KBr diluted discs and a Perkin Elmer MIR-FIR FT-IR spectrometer. Melting points were collected on a Buchi M-560 Melting Point apparatus and are reported uncorrected. Magnetic susceptibility data were collected on microcrystalline samples over a 2-300 K temperature range with an applied field of 1000 Oe using a MPMS SQUID magnetometer. Magnetization studies were performed between 0-7 T at 2 K, 5 K, 7 K and 10 K.

5.2.2. Synthesis of $[Mn(H_2L)(H_2O)_2][Fe(CN)_5(NO)].H_2O$ (15)

To a solution of $[Mn(H_2L)Cl(H_2O)]Cl$ (0.027 mmol, 0.016 g) in 15 mL methanol,

KSCN (0.027 mmol, 0.003 g) was added. The reaction mixture was stirred at room temperature for 3 hours. A solution of $Na_2[Fe(CN)_5NO].2H_2O$ (0.0135 mmol, 0.004 g) in 20 mL distilled water was added without stirring and the resulting solution was kept undisturbed in dark. Brown needle-shaped crystals were observed after 48 hours. The mother liquor was discarded and crystals were washed with ethanol followed by diethyl ether and then air dried. Yield: 0.006 g (71% based on Mn); M. p. >250°C; Elemental analysis: Found C, 50.06%; H, 3.87%; N, 18.65%. $C_{26}H_{26}Fe_{0.5}MnN_{7.5}O_{5.5}$ requires C, 50.83%; H, 4.27%; N, 17.10%. IR (KBr, cm^{-1}): 3411(br), 2141(m), 1891(s), 1616(m), 1536(m), 1488(m), 1367(m), 1298(m), 1152(m), 1047(w), 810(m), 707(m), 413(w).

5.2.3. Synthesis of [{Mn(H$_2$L)}{Fe(CN)$_5$(NO)}] (16)

To a solution of $[Mn(H_2L)Cl(H_2O)]Cl$ (0.027 mmol, 0.016 g) in 15 mL methanol, KSCN (0.027 mmol, 0.003 g) was added. The reaction mixture was stirred at room temperature for 3 hours. 200 mL of distilled water was added and then $Na_2[Fe(CN)_5NO].2H_2O$ (0.0135 mmol, 0.004 g) was added without stirring and kept undisturbed in dark. Brown block shaped crystals were observed after four weeks. The mother liquor was discarded and crystals were washed with ethanol followed by diethyl ether and then air dried. Yield: 0.005 g (62% based on Mn); M. p. >250°C; Elemental analysis: Found: C, 48.97 %; H, 3.03%; N, 22.43%. $C_{28}H_{23}FeMnN_{11}O_4$ requires C, 48.86%; H, 3.37%; N, 22.38%. IR (KBr, cm^{-1}): 3444(br), 2149(m), 1903(s), 1621(m), 1531(m), 1442(m), 1374(m), 1292(m), 1172(m), 1073(w), 1015 (w), 894 (w), 807(m), 696(m), 661 (m), 546(w), 407(s).

5.2.4. Synthesis of [{Mn(H$_2$L)}{Fe(CN)$_5$(NO)}·(H$_2$O)$_{0.75}$]$_n$ (17)

To a solution of $[Mn(H_2L)Cl(H_2O)]Cl$ (0.027 mmol, 0.016 g) in 15 mL methanol, 200 mL distilled water was added. The reaction mixture was stirred at room temperature for 5 min. Then, $Na_2[Fe(CN)_5NO].2H_2O$ (0.0135 mmol, 0.004 g) was added without stirring and kept undisturbed in dark. Yellow needle-shaped crystals were observed after 3 days. The mother liquor was discarded and crystals were washed with ethanol followed by diethyl ether and then air dried. Yield: 0.005 g (60% based on Mn); M. p. >250°C; Elemental analysis: Found: C, 48.82%; H, 3.19%; N, 22.93%. $C_{28}H_{27}FeMnN_{11}O_6$ requires C, 49.20%; H, 3.29%; N, 22.53%. IR (KBr, cm^{-1}):

2959(br), 2156(m), 1906 (m), 1625(m), 1531(w), 1445(w), 1377(w), 1292(m), 1159(w), 810(m), 702(m), 409(s).

5.2.5. Synthesis of $[\{Mn(H_2L)(H_2O)\}_2\{Mn(H_2L)\}\{Fe(CN)_6\}_2].9H_2O$ (18) and $[Mn(H_2L)(H_2O)_2]_2[\{Mn(H_2L)(H_2O)\}_2\{Fe(CN)_6\}][\{Mn(H_2L)\}_2\{Fe(CN)_6\}_3].13H_2O$ (19)

To a solution of $[Mn(H_2L)(H_2O)Cl]Cl$ (0.03 mmol, 0.0180 g) in 10 mL ethanol, $NaClO_4.H_2O$ (0.015 mmol, 0.0021 g) dissolved in 1 mL distilled water was added. Stirring was continued for an hour at room temperature. Then, the reaction mixture was diluted with 50 mL of distilled water followed by the addition of aqueous solution of $K_3[Fe(CN)_6]$ (0.015 mmol, 0.0049 g) without agitation. The reaction mixture was kept undisturbed for slow evaporation at room temperature in dark. Yellow plate shaped crystals of compound **18** are observed after 24 hours. Crystals of compound **18** were isolated and the mother liquor was left undisturbed in dark. Yellow needle shaped crystals of compound **19** were observed after 72 hours. The mother liquor was discarded and crystals were extracted, washed with ethanol and diethyl ether and air dried. Characterization data for **18**: Yield: 0.011 g (55 % based on Mn); M. p. >250°C; Elemental analysis: Found C, 49.47%; H, 4.23%; N, 19.27%. $C_{81}H_{85}N_{27}O_{17}Mn_3Fe_2$ requires C, 49.01%; H, 4.32%; N, 19.05%. IR (KBr, cm^{-1}): 3402(br), 2377(s), 2116(m), 1622(s), 1527(m), 1484(m), 1375(w), 1286(s), 1167(s), 1075(m), 1017(w), 810(m), 700(m), 411(m). Characterization data for **19**: Yield: 0.006 g (29 % based on Mn); M. p. >250°C; Elemental analysis: Found C, 50.80%; H, 3.32%; N, 19.01%. $C_{137}H_{147}N_{47}O_{31}Mn_5Fe_4$ requires C, 50.31%; H, 2.97%; N, 19.57%. IR (KBr, cm^{-1}): 3398(br), 2115(s), 1625(s), 1524(m), 1440(m), 1379(w), 1284(s), 1172(s), 1079(m), 895(w), 809(m), 706(m), 432(w).

5.2.6. Single Crystal X-Ray Diffraction Studies

Suitable single crystals of all the compounds obtained directly from the reaction mixtures were used for diffraction measurements. The diffraction data for the compounds were collected on a Bruker APEX-II CCD diffractometer using MoKα radiation (λ=0.71073 Å) using φ and ω scans of narrow (0.5°) frames at 90-100K. All the structures were solved by direct methods using SHELXL-97 as implemented in the

WinGX program system [49]. Anisotropic refinement was executed on all non-hydrogen atoms. The aliphatic and aromatic hydrogen atoms were placed on calculated positions but were allowed to ride on their parent atoms during subsequent cycles of refinements. Positions of N-H and O-H hydrogen atoms were located on a difference Fourier map and allowed to ride on their parent atoms during subsequent cycles of refinements. Crystallographic data (excluding structure factors) have been deposited with the Cambridge Crystallographic Data Centre, CCDC, 12 Union Road, Cambridge CB21EZ, UK. Copies of the data can be obtained free of charge on quoting the depository number CCDC 993506 (**15**), CCDC 993117 (**16**), CCDC 1009780 (**17**) and CCDC 1489308 (**18**). The crystal data and refinement parameter of compounds **15-19** are listed in Table 5.2.

Continuous SHAPE analysis of the coordination environment around the central Mn(II) center was performed [50]. The results obtained from careful shape analysis are listed in Table 5.1.

Table 5.1. Shape analysis data for compounds **15-19** using SHAPE program

Complex	HP-7	HPY-7	PBPY-7	COC-7	CTPR-7	JPBPY-7	JETPY-7
15	32.066	20.222	0.951	6.366	4.684	3.944	20.288
16	32.751	24.543	0.558	8.259	6.207	3.575	23.446
17 (Mn1)	31.731	22.867	0.850	6.844	4.950	3.994	19.147
17 (Mn2)	32.214	20.610	1.288	7.259	4.989	4.297	17.722
18 (Mn1)	31.329	21.313	0.823	6.876	5.347	3.771	19.435
18 (Mn2)	30.306	32.423	0.447	8.312	8.470	1.853	38.459
19 (Mn1)	32.541	24.274	0.439	7.340	5.647	3.824	23.133
19 (Mn2)	33.220	23.002	0.510	7.611	5.774	3.618	22.106

HP-7:Heptagon (D_{7h}); HPY-7:Hexagonal pyramid (C_{6v}); PBPY-7:Pentagonal bipyramid (D_{5h}); COC-7:Capped octahedron (C_{3v}); CTPR-7: Capped trigonal prism (C_{2v}); JPBPY-7: Johnson pentagonal bipyramid J13 (D_{5h}); JETPY-7: Johnson elongated triangular pyramid J7 (C_{3v}).

5.3. Results and Discussions

5.3.1. Synthesis and characterization of $[Mn(H_2L)(H_2O)_2][Fe(CN)_5(NO)].H_2O$ (15)

Reaction of $[Mn(H_2L)(H_2O)Cl]Cl$ with $[Fe(CN)_5(NO)]^{3-}$ in aqueous methanolic medium immediately leads to the formation of an amorphous solid, which is insoluble

Table 5.2. Crystal data and refinement parameters of compounds **15**-**19**

Complex	**15**	**16**	**17**	**18**	**19**
Empirical formula	$C_{52}H_{52}N_{15}O_{11}FeMn_2$	$C_{28}H_{23}N_{11}O_4FeMn$	$C_{84}H_{67}N_{33}O_{11.25}Fe_3Mn_3$	$C_{81}H_{61}N_{27}O_{23}Fe_2Mn_3$	$C_{162}H_{114}N_{54}O_{31}Fe_4Mn_6$
Formula weight	1228.82	688.36	4102.09	2057.09	3866.11
CCDC	993506	993117	1009780	1489308	-
Temperature/K	100	100	100	296	100
Crystal system	Triclinic	Monoclinic	Triclinic	Monoclinic	Triclinic
Space group	*P-1*	*$P2_1/c$*	*P-1*	*C2/c*	*P-1*
a/Å	9.782 (3)	8.888 (4)	10.317 (8)	32.757 (2)	10.323 (15)
b/Å	10.001 (3)	17.128 (8)	17.425 (15)	16.903(7)	15.691 (2)
c/Å	15.302 (4)	20.021 (9)	26.010 (2)	18.219(9)	29.469 (4)
α/°	87.20 (1)	90.00	77.31 (6)	90.00	103.34 (4)
β/°	77.81 (1)	96.28 (2)	84.36 (5)	96.70 (2)	97.14 (4)
γ/°	72.72 (1)	90	85.21 (5)	90.00	95.14 (4)
Volume/$Å^3$	1397.1 (7)	3029.8 (2)	4530.7 (6)	10019 (7)	4538.8 (8)
Z	1	4	1	4	1
ρ_{calc}, g cm^{-3}	1.460	1.509	1.503	1.364	1.404
μ/mm^{-1}	0.774	0.949	0.952	0.730	0.789
Crystal size, mm^3	0.47x0.08x0.03	0.36x0.32x0.16	0.16x0.10x0.04	0.14x0.10x0.08	0.38x0.12x0.08
F(000)	633	1404	2086	4188	1966
Data/parameters/restraints	5367/410/20	7126/424/0	20667/1246/3	9349/639/0	9552/1171/12
Goodness-of-fit on F^2	0.885	1.095	0.862	1.023	1.049
Final R indexes [I>=2σ (I)]	R_1= 0.0410 ; wR_2=0.0811	R_1= 0.0320 ; wR_2=0.0913	R_1= 0.1133 ; wR_2=0.1282	R_1= 0.0960 ; wR_2=0.2290	R_1= 0.0819; wR_2=0.1966
Final R indexes [all data]	R_1= 0.0921; wR_2=0.0978	R_1= 0.0379; wR_2=0.1047	R_1= 0.3004 ; wR_2=0.1654	R_1= 0.1846; wR_2=0.2833	R1= 0.1409; wR_2=0.2350

in common organic solvents. Therefore, in order to prevent the formation of any polymeric material, initial investigation of the self-assembly between PBP Mn(II) complex $[Mn(H_2L)Cl(H_2O)]Cl$ with nitroprusside anion was carried out in presence of KSCN.

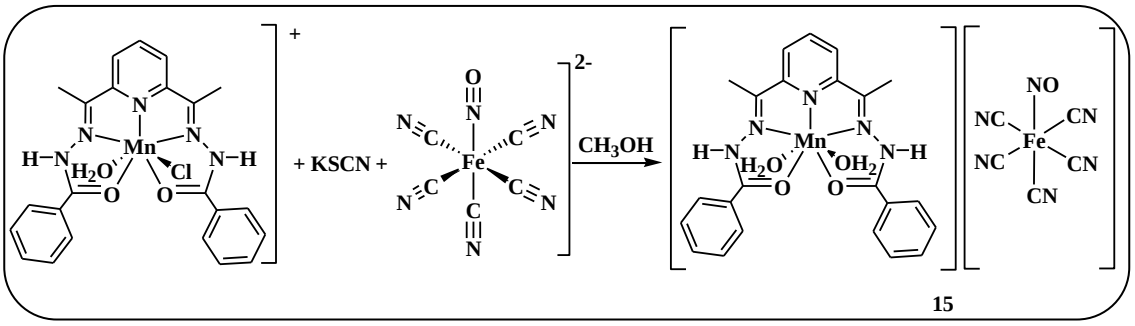

Scheme 5.1. Synthesis of compound **15**

It was anticipated that KSCN will coordinate to one of the axial sites of $[Mn(H_2L)Cl(H_2O)]Cl$ and thus prevent formation of polymeric species. Reaction of $Na_2[Fe(CN)_5(NO)]$ with $[Mn(H_2L)Cl(H_2O)]Cl$ in presence of KSCN resulted in the formation of $[Mn(H_2L)(H_2O)_2][Fe(CN)_5(NO)].H_2O$ (**15**) as yellow single crystalline product (Scheme 5.1). Contrary to our anticipation, SCN^- failed to coordinate to the axial sites of $[Mn(H_2L)]^{2+}$. Instead, the nitroprusside ion is present as an anion, thereby maintaining the charge neutrality of the compound. However, isolation of a molecular

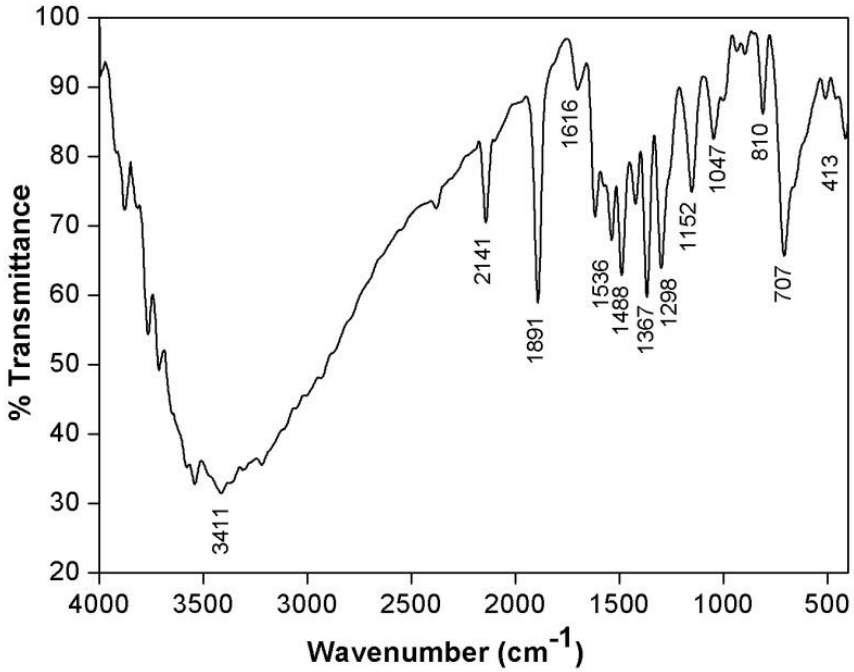

Figure 5.1. FT-IR spectrum of compound **15** as KBr diluted discs

species indicates the competing character of KSCN in the self assembly process. The lack of cyano bridges in compound **15** can be primarily attributed to the rapid crystallization of the ionic pair. Compound **15** was characterized with the help of elemental analysis, FT-IR and single crystal X-ray diffraction studies.

Results of elemental analysis are in good agreement with the proposed formulation of compound **15**. The IR spectrum of compound **15** recorded as KBr disc is depicted in Figure 5.1. The spectrum features strong absorption at 2141 cm^{-1}, which can be easily assigned to C≡N stretching vibration of the nitroprusside anion. Another strong band was observed at 1891 cm^{-1}. This band can be attributed to N=O stretching vibration and it indicates the presence of nearly linear Fe-N-O linkages of the nitroprusside moiety. Moreover, C=N stretching vibration of the imine group from ligand H_2L is observed at 1616 cm^{-1} as an intense band. The absorption peak at 1536 cm^{-1} is due to the phenyl ring present in the ligand H_2L moiety.

5.3.2. Molecular structure of compound 15

Single crystal X-ray structural analysis of compound **15** reveals that it crystallizes in triclinic P-1 space group with one lattice water molecule. Important bond lengths and bond angles are listed in Table 5.3. Compound **15** comprises of one $[Mn(H_2L)(H_2O)_2]^{2+}$ cation and one $[Fe(CN)_5(NO)]^{2-}$ anion (Figure 5.2). It was initially anticipated that cyano groups from nitroprusside anion will bridge the cationic $[Mn(H_2L)]^{2+}$ unit at the axial coordination sites and thus result in heterobimetallic aggregate. However, compound **15** lacks any such interconnection and can be visualized as a simple

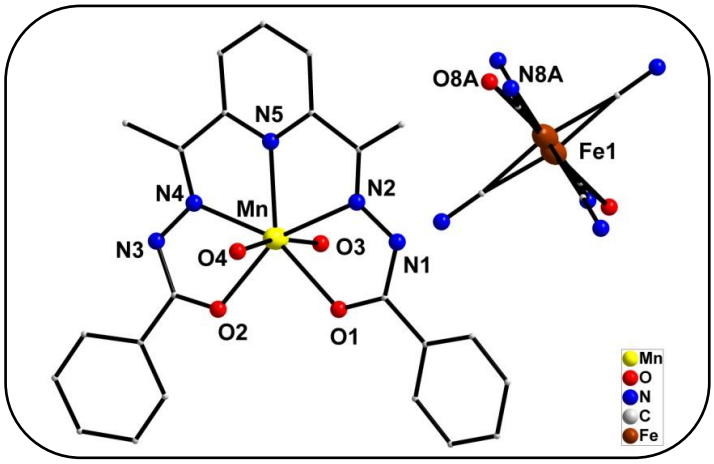

Figure 5.2. Molecular structure of compound **15**. Lattice solvents and hydrogen atoms are omitted for clarity

bimetallic salt formed by cationic $[Mn(H_2L)(H_2O)_2]^{2+}$ and anionic $[Fe(CN)_5(NO)]^{2-}$. Mn(II) atom in compound **15** is heptacoordinated with five of its equatorial coordination sites occupied by donor atoms from the planar pentadentate ligand. The two axial positions of Mn(II) are occupied by O atoms from coordinated H_2O groups and thus the Mn(II) center acquires distorted PBP geometry with a N_3O_4 coordination environment. Although the absence of cyano bridges in compound **15** initially appears unusual, several bimetallic ionic pair compounds featuring cationic Mn(II) complex ion and nitroprusside anion have been reported earlier [51]. The axial Mn-O(H_2O) distances measure 2.146(2) Å and 2.252(2) Å. These values compare well with Mn-O(H_2O) distances observed in ionic bimetallic nitroprusside based Mn(II) complex reported earlier [51]. The Fe(II) ions of nitroprusside anions in compound **15** possesses

Table 5.3. Selected bond lengths [Å] and angles [°] for compound **15**

Mn(1)-O(3)	2.146(2)	O(2)-Mn(1)-O(3)	90.01(8)
Mn(1)-O(2)	2.208(2)	O(4)-Mn(1)-O(3)	167.83(9)
Mn(1)-O(4)	2.252(2)	O(4)-Mn(1)-O(2)	85.81(8)
Mn(1)-N(4)	2.264(2)	N(4)-Mn(1)-O(3)	93.91(9)
Mn(1)-N(5)	2.272(2)	N(4)-Mn(1)-O(2)	69.11(7)
Mn(1)-O(1)	2.2997(2)	O(4)-Mn(1)-N(4)	95.26(8)
Mn(1)-N(2)	2.344(2)	N(5)-Mn(1)-O(3)	101.24(9)
O(4)-H(4A)	0.86(3)	N(5)-Mn(1)-O(2)	137.78(7)
O(4)-H(4B)	0.84(4)	N(5)-Mn(1)-O(4)	89.46(8)
N(4)-C(15)	1.289(3)	N(5)-Mn(1)-N(4)	69.61(8)
N(4)-N(3)	1.386(3)	O(1)-Mn(1)-O(3)	84.75(8)
C(8)-N(2)	1.282(3)	O(1)-Mn(1)-O(2)	86.63(7)
N(2)-N(1)	1.384(3)	O(1)-Mn(1)-O(4)	83.60(8)
N(1)-C(7)	1.355(4)	O(1)-Mn(1)-N(4)	155.70(8)
N(1)-H(1A)	0.84(3)	O(1)-Mn(1)-N(5)	134.49(8)
N(3)-C(17)	1.338(4)	N(2)-Mn(1)-O(3)	92.72(8)
C(14)-N(5)	1.344(3)	N(2)-Mn(1)-O(2)	152.92(7)
N(5)-C(10)	1.335(3)	O(4)-Mn(1)-N(2)	85.92(8)
C(24)-Fe(1)	1.990(6)	N(2)-Mn(1)-N(4)	137.40(8)

a distorted octahedral geometry with approximate C_{4v} symmetry. It is coordinated by five carbon atoms of cyano ligand and a nitrogen atom from nitrosyl ligand. The average Fe-C distance is 1.859(6) Å while the average Fe-N distance is 1.939(7) Å. The nitroprusside anion is present in a special position and only one half of the nitroprusside anion is present in the asymmetric unit while the other half is symmetry generated. This creates ambiguity in assigning the exact position of the nitrosyl group within the nitroprusside anion as there is only one nitrosyl group. Moreover, the CN and NO groups appear at the same position because of positional disorder. Terminal nitrogen atom of cyano group N(8) and oxygen atoms of NO groups, O(8) are modelled with 50% site occupancy factor. However, the linked C atoms of cyano group and N atoms of nitrosyl groups are not modelled and kept as 100% occupancy of carbon C(26). However, both C(26) atoms should have 50% site occupancy factor of carbon and nitrogen. The $[Mn(H_2L)(H_2O)_2]^{2+}$ cation, $[Fe(CN)_5(NO)]^{2-}$ anion and lattice water molecule in compound **15** are involved in extensive hydrogen bonding and a perspective view of H-bonding network present in compound **15** is depicted in Figure 5.3. Hydrogen atoms, H(4A) and H(4B) atoms from one of the coordinated water

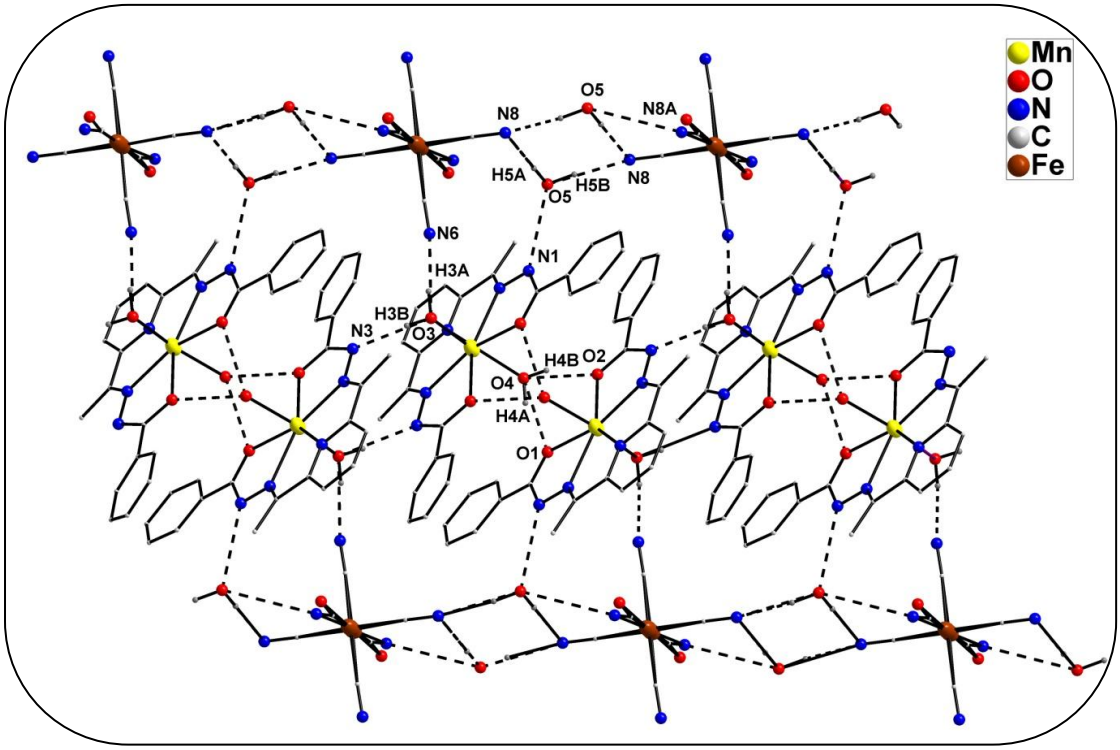

Figure 5.3. Hydrogen bonded network present in compound **15**

molecule O(4) in $[Mn(H_2L)(H_2O)_2]^{2+}$ cation are involved in H-bonding with the ligand oxygen O(1) and O(2) atoms in a neighbouring $[Mn(H_2L)(H_2O)_2]^{2+}$. This leads to the formation of a moderately strong (mean donor-acceptor distances measure 2.756 Å H-bonded $[Mn(H_2L)(H_2O)_2]_2$ dimeric units. Hydrogen atoms H(3B) from the remaining coordinated water (O(3)) molecule in this dimer are involved in hydrogen bonding with N(6) atoms of neighbouring nitroprusside anions (O(3)–H(3B)···N(6)) distance measure 2.877(3) Å). H(1A) atom attached to the hydrazide nitrogen atoms, N(1) is H-bonded with oxygen O(5) atom from lattice water molecule.

Moreover, the hydrogen atoms, H(5A) and H(5B) of lattice water molecules are H-bonded with N(8) atom from nitroprusside anion. This leads to the formation of a nearly planer square shaped eight member ring as shown in Figure 5.3. The mean donor acceptor distance of the hydrogen bonds formed by water molecules measure 3.033 Å. This hydrogen bonding interaction of compound **15** resulted in the formation of 2D network throughout the plane. The hydrogen bonded parameters are listed in Table 5.4.

Table 5.4. Hydrogen bonding parameters of compound **15**

Interaction	**H···A (Å)**	**D···A (Å)**	**∠D–H···A (°)**	**Symmetry**
N1–H1A···O5	2.18	2.999 (3)	163.9	x,y,z
O3–H3A···N3	1.98	2.827 (3)	172.6	-x+1,-y,-z+2
O5–H5B···N8	1.96	2.898 (5)	166.8	x+1,+y,+z
O4–H4A···O1	1.97	2.795 (3)	158.6	-x+1,-y+1,-z+2
O4–H4B···O2	1.94	2.717 (3)	153.5	-x+1,-y+1,-z+2
O3–H3B···N6	1.96	2.877 (3)	173.7	-x+1,-y+1,-z+1
O5–H5A···N8	2.26	3.203 (4)	174.4	-x+1,-y+1,-z+1

5.3.3. Synthesis and characterization of $[\{Mn(H_2L)\}\{Fe(CN)_5(NO)\}]$ (16)

Since the reaction of $[Mn(H_2L)Cl(H_2O)]Cl$ with $[Fe(CN)_5(NO)]^{2-}$ in presence of KSCN resulted in the formation of an ionic species with no cyano linkage, the same reaction was carried out in presence of excess water. When the reaction of $Na_2[Fe(CN)_5(NO)]$ with $[Mn(H_2L)Cl(H_2O)]Cl$ and KSCN was carried out in the presence of excess water, it resulted in the formation of a dimeric complex $[\{Mn(H_2L)\}\{Fe(CN)_5(NO)\}]$ (**16**). As anticipated, excess water helped to keep the ionic species in solution and favour the

formation of compound **16** with cyano bridges. Thus, dark brown block shaped crystals of compound **16** were obtained after one month (Scheme 5.2).

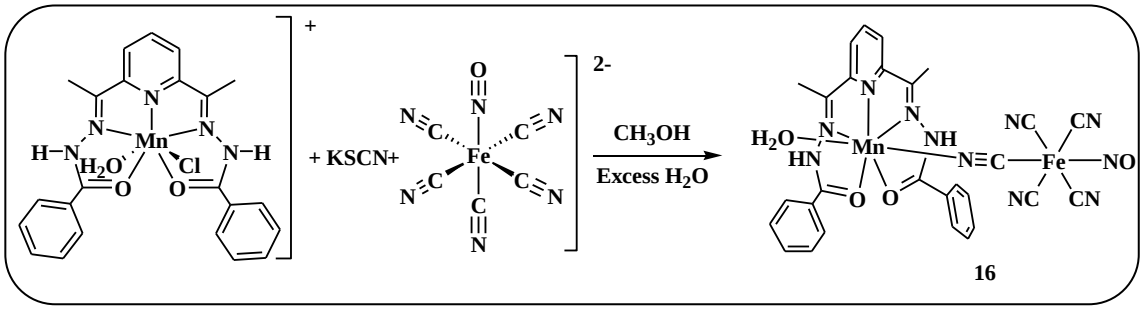

Scheme 5.2. Synthesis of compound **16**

Compound **16** was also characterized with the help of elemental analysis, FT-IR and single crystal X-ray diffraction studies. The elemental analysis data obtained agrees well with the calculated data of the proposed formulation of compound **16**. The FT-IR spectrum of compound **16** is depicted in Figure 5.4. Strong absorptions at 1903 cm^{-1} and 2149 cm^{-1} in the IR spectrum of compound **16** as KBr disc, are attributed to N=O and C≡N stretching vibrations of the nitroprusside anion. Another strong absorption observed at 1621 cm^{-1} can be assigned to C=N stretching vibration of the imine group from the ligand. The absorption peak at 1531 cm^{-1} is due to the presence of the phenyl rings.

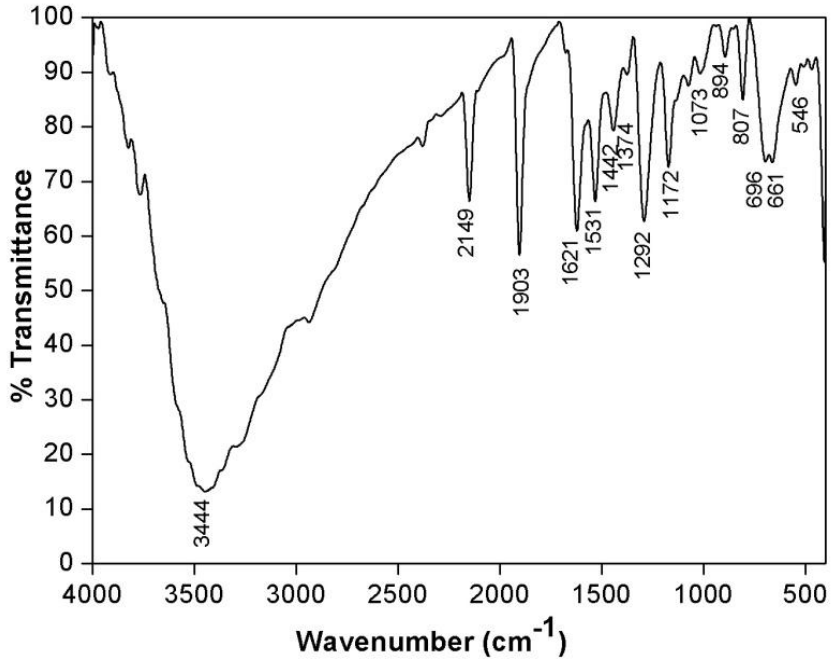

Figure 5.4. FT-IR spectrum of compound **16** as KBr diluted discs

5.3.4. Molecular structure of compound 16

Single crystal X-ray diffraction analysis reveals that compound **16** crystallizes in monoclinic $P2_1/c$ space group. Molecular structure of compound **16** depicted in Figure 5.5 clearly reveals the formation of a cyano-bridged Mn(II)-Fe(II) binuclear species. Important bond lengths and bond angles are listed in Table 5.5. Mn(II) atom in compound **16** retains the hepta-coordinated PBP geometry present in the precursor complex. The planar pentadentate ligand occupy the five equatorial sites of the Mn(II) centre as in the case of the precursor complex. One of the axial positions of the PBP Mn(II) unit is linked to the $[Fe(CN)_5(NO)]^{2-}$ unit via a cyanide N atom. The other axial site of Mn(II) atom is occupied by a coordinated water molecule and thus prevent the formation of higher nuclearity aggregates through further bridging.

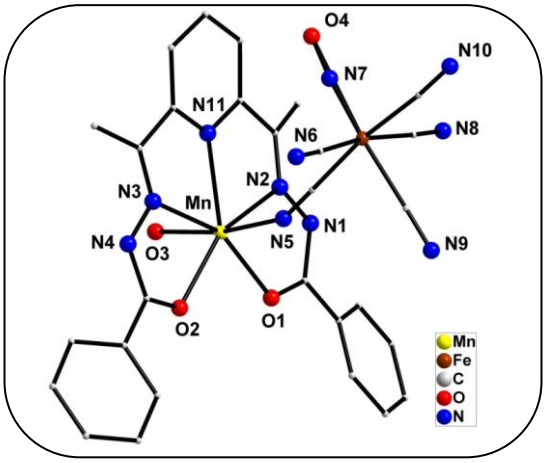

Figure 5.5. Molecular structure of compound **16**. Lattice solvents and hydrogen atoms are omitted for clarity

Thus, Mn(II) atom in compound **16** has a N_4O_3 coordination environment with a distorted PBP geometry. The Mn(II)-Fe(II) separation in compound **16** is found to be 5.134 Å. Several heterobimetallic Mn(III)-nitroprusside aggregates have been reported in literature [52-57]. Intriguingly, apart from $[Mn(bpy)_2(H_2O)][FeCN)_5(NO)].H_2O$, compound **16** represent the only example of bimetallic Mn(II)-nitroprusside aggregate where cyano group of nitroprusside unit is coordinated to Mn(II) [58]. Hydrogen atoms, H(3A) and H(3B) from the axial water O(3) molecule coordinated to Mn(II) in compound **16** are involved in hydrogen bonding with nitrogen atoms, N(9) and N(10) of two neighbouring molecules. This leads to the formation of a O-H···N H-bonded 2D network with mean donor acceptor distance measuring 2.890 Å. These 2D networks are

further interconnected by N-H···N hydrogen bonding leading to the formation of a 3D supramolecular assembly. The 3D assembly of the compound **16** formed through hydrogen bond is depicted in Figure 5.6. The hydrogen bonding parameters of compound **16** are listed in Table 5.6. While viewing from another plane, the linkages between the consecutive planes are observed. The N(1) and N(6) atoms of the two planes are H-bonded, giving rise to the 3D network of the compound. (Figure 5.7).

Table 5.5. Selected bond lengths [Å] and angles [°] for compound **16**

Mn(1)-O(3)	2.2131(12)	O(3)-Mn(1)-N(5)	171.35(5)
Mn(1)-N(5)	2.2135(14)	O(2)-Mn(1)-O(3)	94.11(5)
Mn(1)-O(2)	2.2652(12)	O(2)-Mn(1)-N(5)	91.74(5)
Mn(1)-O(1)	2.2678(12)	O(1)-Mn(1)-O(3)	87.91(5)
Mn(1)-N(2)	2.3086(15)	O(1)-Mn(1)-N(5)	98.72(5)
Mn(1)-N(11)	2.3091(14)	O(1)-Mn(1)-O(2)	87.48(4)
Mn(1)-N(3)	2.3228(14)	O(3)-Mn(1)-N(2)	84.97(5)
Fe(2)-N(7)	1.6558(16)	N(2)-Mn(1)-N(5)	92.20(5)
Fe(2)-C(27)	1.9355(19)	O(2)-Mn(1)-N(2)	156.36(5)
Fe(2)-C(29)	1.9429(16)	O(3)-Mn(1)-N(11)	84.36(5)
Fe(2)-C(25)	1.9451(17)	N(5)-Mn(1)-N(11)	87.00(5)
Fe(2)-C(28)	1.9516(17)	O(2)-Mn(1)-N(11)	135.59(5)
C(10)-N(11)	1.342(2)	O(1)-Mn(1)-N(11)	136.59(5)
C(14)-N(11)	1.344(2)	N(2)-Mn(1)-N(11)	67.92(5)
N(1)-N(2)	1.378(2)	O(3)-Mn(1)-N(3)	91.91(5)
N(3)-N(4)	1.3756(20)	O(2)-Mn(1)-N(3)	68.52(5)
N(7)-O(4)	1.143(2)	N(2)-Mn(1)-N(3)	135.08(5)

Table 5.6. Hydrogen bonding parameters of compound **16**

Interaction	**H···A (Å)**	**D···A (Å)**	**∠D–H···A(°)**	**Symmetry**
N4–H4A···N8	2.04	2.876 (2)	168.1	-x+1,+y-1/2,-z+1/2
O3–H3A···N9	2.15	2.918 (2)	179.3	x,-y+1/2+1,+z-1/2
N1–1A···N6	2.12	2.933 (2)	167.3	-x+1,+y+1/2,-z+1/2
O3–H3B···N10	2.04	2.863 (2)	168.4	x-1,-y+1/2+1,+z-1/2

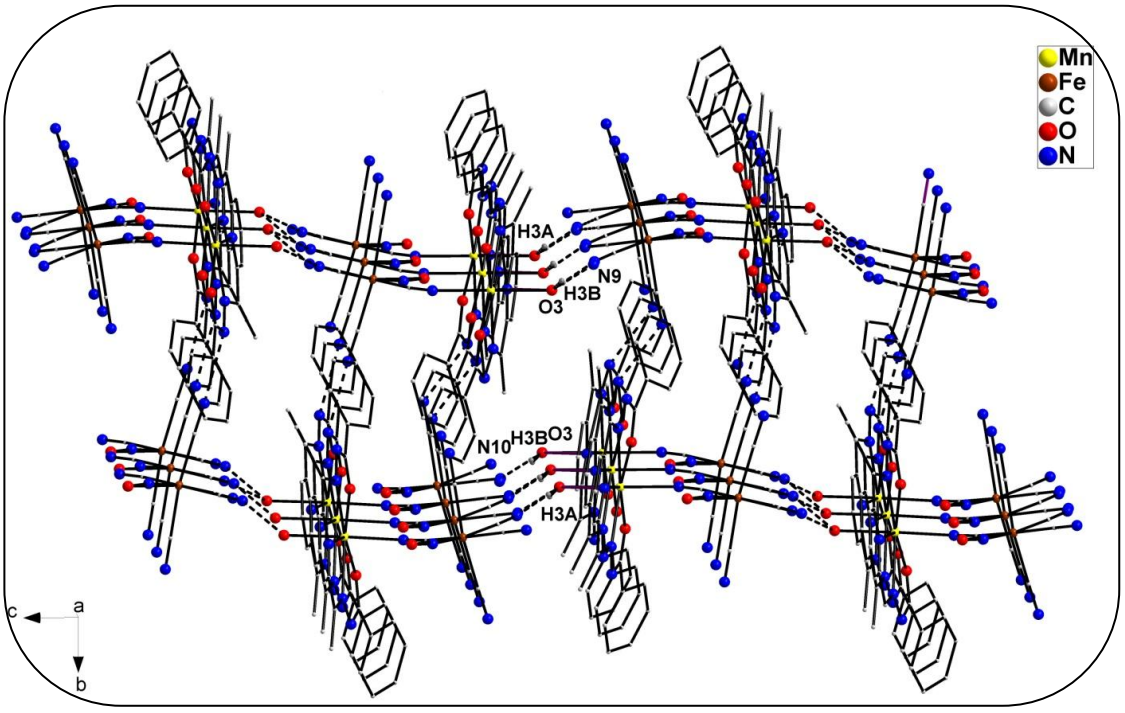

Figure 5.6. O-H···N-bonded network present in compound **16**. Aromatic and aliphatic hydrogen atoms are omitted for clarity

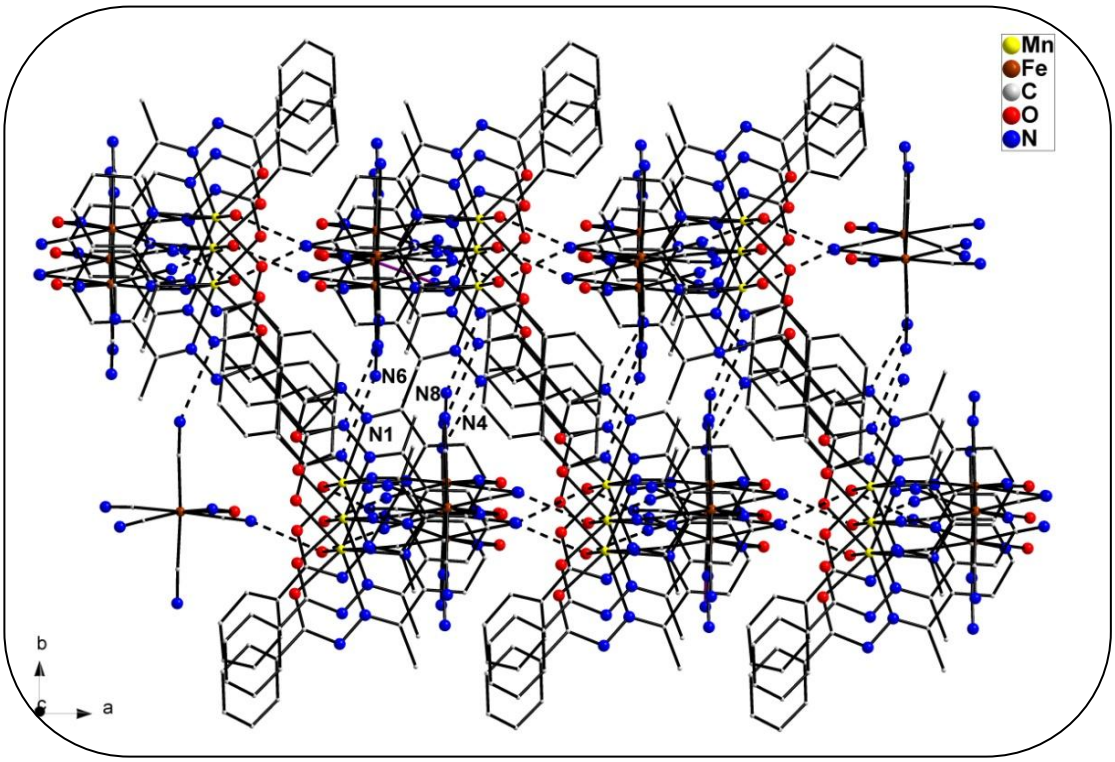

Figure 5.7. N-H···N hydrogen bonded network present in compound **16**. Aromatic and aliphatic hydrogen atoms are omitted for clarity

5.3.5. Synthesis and characterization of $[\{Mn(H_2L)\}\{Fe(CN)_5(NO)\}\cdot(H_2O)_{0.75}]_n$ (17)

Although in case of compounds **15** and **16**, KSCN did not coordinate to the Mn(II) ion in the final product, its influence was evident as nitroprusside did not link both the axial sites. It was anticipated that higher nuclearity Mn(II)-Fe(II) species can be possibly obtained if both the axial coordination site of $[Mn(L)]^{2+}$ are linked by nitroprusside anions. Therefore, when the reaction of $Na_2[Fe(CN)_5(NO)]$ with $[Mn(H_2L)Cl(H_2O)]Cl$ was carried out in absence of KSCN, it resulted in the formation of $[\{Mn(H_2L)\}\{Fe(CN)_5(NO)\}\cdot(H_2O)_{0.75}]_n$ (**17**) as yellow needle shaped crystals. The crystals of compound **17** were isolated in good yield from the above reaction mixture (Scheme 5.3).

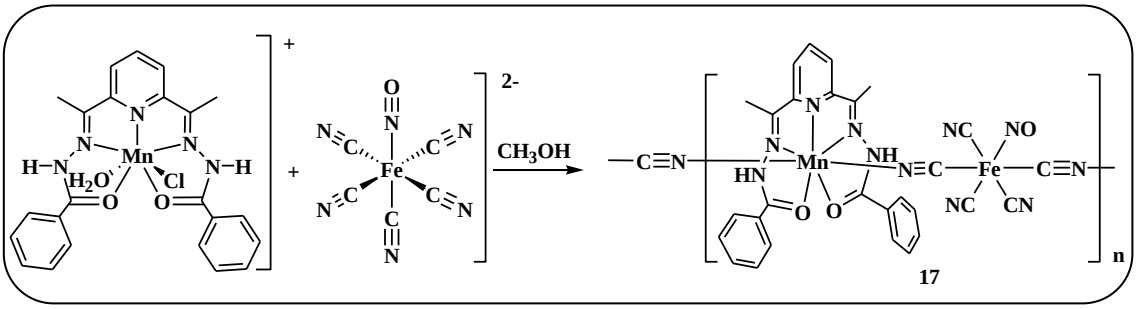

Scheme 5.3. Synthesis of compound **17**

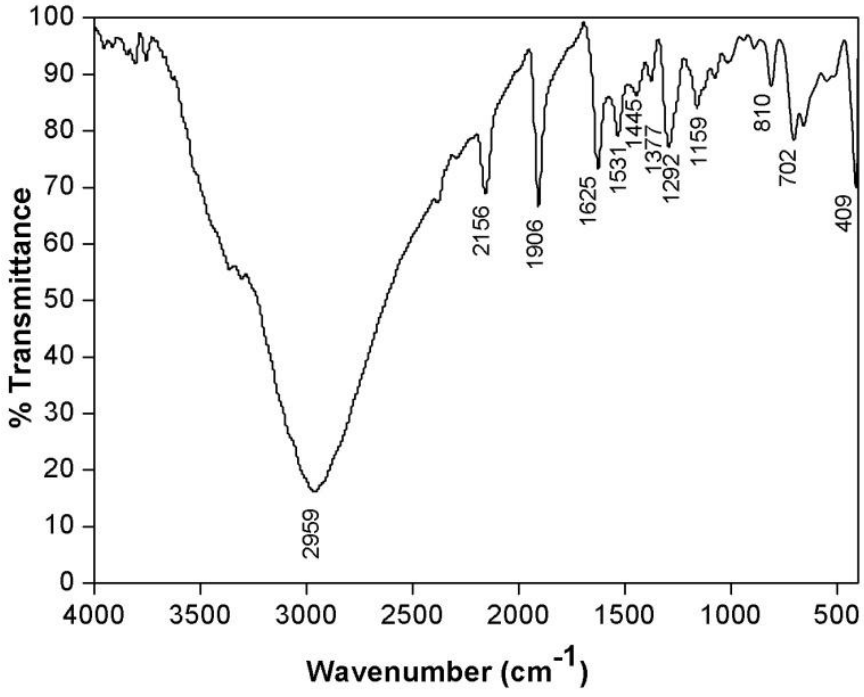

Figure 5.8. FT-IR spectrum of compound **17** as KBr diluted discs

The synthesized compound was characterized by elemental analysis, FT-IR and single crystal X-ray diffraction studies. The data obtained from elemental analysis agrees well with the calculated data of the proposed composition of compound **17**. The FT-IR spectrum of compound **17** as KBr disc is depicted in Figure 5.8. The spectrum features strong absorptions peaks at 2156 cm^{-1} and 1906 cm^{-1} which can be easily assigned to C≡N and N=O stretching vibrations respectively. The C=N stretching vibration of the imine group of H_2L ligand is observed as strong absorption at 1625 cm^{-1}. The stretching frequency due the phenyl ring is observed at 1531 cm^{-1}.

5.3.6. Molecular structure of compound 17

Single crystal X-ray diffraction measurement was carried out to unambiguously establish the crystal structure of compound **17**. It crystallizes in P-1 space group. A perspective view of the crystal structure of compound **17** is depicted in Figure 5.9.

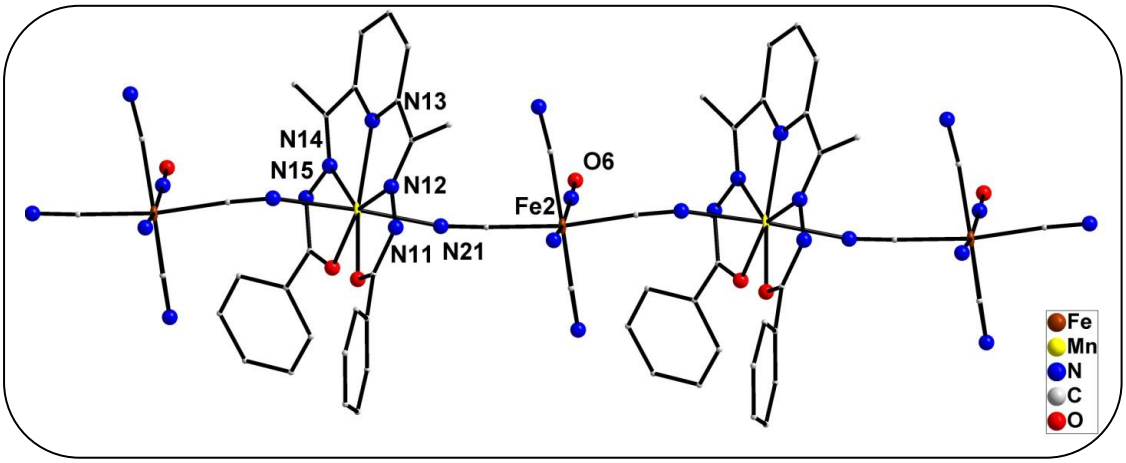

Figure 5.9. Molecular structure of compound **17**. Aromatic and aliphatic hydrogen atoms are omitted for clarity

Compound **17** has a chain like structure formed by alternate $[Mn(H_2L)]^{2+}$ and $[Fe(CN)_5(NO)]^{2-}$ moieties. As in case of compounds **15** and **16**, Mn(II) atom in compound **17** is also heptacoordinated with a PBP geometry. While the equatorial coordination sites of Mn(II) are occupied by N_3O_2 donor atoms of the bishydrazone ligand. Both the axial coordination sites of the Mn(II) atom are occupied by N atoms of the cyano groups of neighbouring nitroprusside anions. This eventually leads to the formation of an electro-neutral 1D polymeric chain structure in compound **17** as shown in Figure 5.9. The important bond lengths and bond angles of compound **17** are listed in

Table 5.7. Careful shape analysis of the compound reveals that pentagonal bipyramidal coordination environment is maintained around the Mn((II) centres. The data obtained by using SHAPE program is listed in Table 5.1.

Table 5.7. Selected bond lengths [Å] and angles [°] for compound **17**

Fe(1)-N(11)	1.653 (4)	N(11)-Fe(1)-C(24)	97.67 (2)
Fe(1) -C(24)	1.929 (5)	C(24)-Fe(1)-C(25)	86.67 (2)
Fe(1) -C(25)	1.939 (5)	N(22)- Fe(2)-C(53)	92.86 (2)
Fe(1) -C(26)	1.923 (5)	C(53)-Fe(2)-C(56)	166.99 (2)
Fe(1) -C(27)	1.939 (4)	C(53)-Fe(2)-C(54)	81.94 (2)
Mn(1)-O(2)	2.221 (3)	C(53)-Fe(2)-C(55)	89.52 (2)
Mn(1)-N(2)	2.319 (4)	C(56)-Fe(2)-C(54)	85.51 (2)
Mn(1)-N(6)	2.195 (4)	C(56)-Fe(2)-C(52)	91.24 (2)
O(4)- C(29)	1.242 (6)	C(54)-Fe(2)-C(52)	82.91 (2)
O(3)-N(11)	1.152 (6)	C(52) -Fe(2)-C(55)	171.88 (2)
N(23)-N(24)	1.363 (5)	N(33)-Fe(3)-C(82)	175.35 (2)
N(23)-C(57)	1.364 (7)	Fe(1)-N(11)-O(3)	174.61 (4)
N(8)-C(26)	1.172 (7)	O(2) -Mn(1)-N(3)	134.80 (1)
N(2)-N(1)	1.379 (5)	O(1)-Mn(1)-N(2)	68.58 (1)
N(3)-C(10)	1.332 (6)	N(3)-Mn(1)-N(6)	92.34 (2)
N(3)-C(14)	1.344 (6)	O(4)-Mn(2)-O(5)	85.24 (1)
O(6)-N(22)	1.154 (7)	O(5)-Mn(2)-N(17)	89.22 (2)

The N-H hydrogen atoms are H-bonded to N/O atom of nitroprusside unit from nearby chains and thus leads to the formation of an interesting supramolecular architecture. The hydrogen atoms attached to N(26) and N(11) i.e., H(26A) and H(11A) are bonded to the nitrogen atoms, N(7) and N(9) respectively of the nitroprusside units. These H-bonding interactions bridge three nearby 1D chain as shown in Figure 5.10 and the hydrogen bonding parameters are listed in Table 5.8. The remaining N-H atoms of [Mn(H_2L)] units within the triple chains are involved in extensive H-bonding with hydrogen atoms of lattice water molecules. This leads to the formation of a 2D sheet like supramolecular network in compound **17** (Figure 5.10).

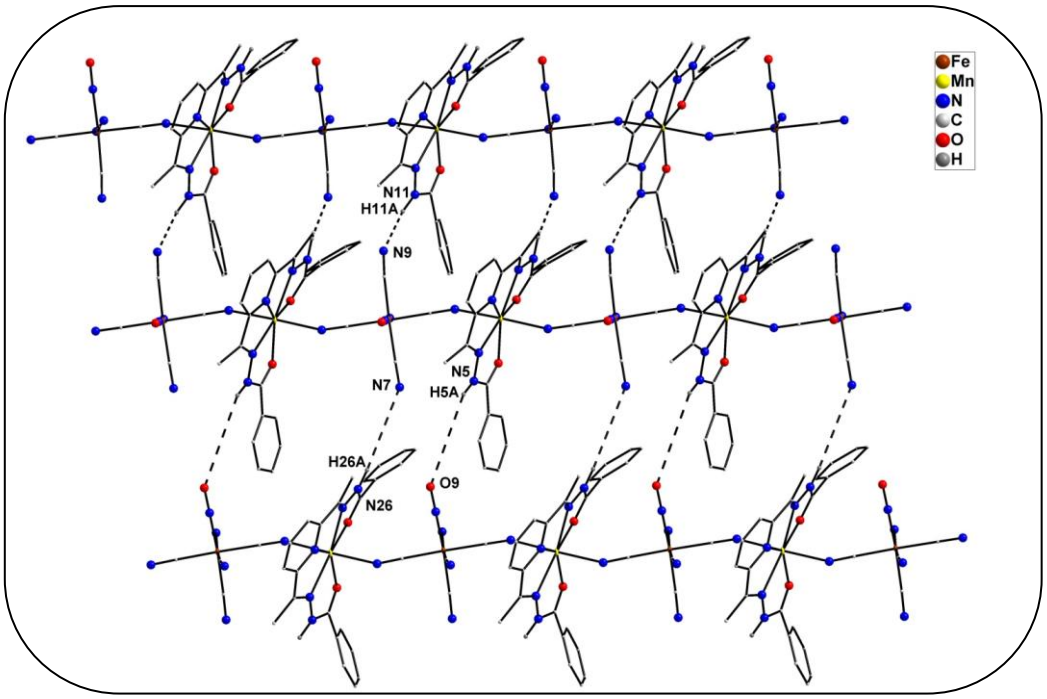

Figure 5.10. N-H···N and N-H···O hydrogen bonding network in compound **17**

Table 5.8. Hydrogen bonding parameters of compound **17**

Interaction	**H···A (Å)**	**D···A (Å)**	**∠D–H···A (°)**	**Symmetry**
N(23)–H(23A)···O(11)	1.83	2.794 (6)	168.2	x,y,z
N(12)–H(12A)···N(32)	2.10	2.969 (6)	171.4	x-1,+y,+z
O(10)–H(10A)···N(29)	2.07	2.848 (7)	179.6	x-1,+y,+z
N(1)–H(1A)···N(21)	1.98	2.984 (6)	171.2	x-1,+y+1,+z
O(10)–H(10B)···N(8)	2.19	3.017 (6)	169.7	-x+1,-y+1,-z+1
N(5)–H(5A)···O(10)	1.98	2.965 (6)	168.9	x,+y,+z+1
O(11)–H(11A)···N(10)	2.03	2.860 (5)	161.0	x,+y,+z-1

5.3.7. Synthesis and characterization of $[\{Mn(H_2L)(H_2O)\}_2\{Mn(H_2L)\}\{Fe(CN)_6\}_2].9H_2O$ (18) and $[Mn(H_2L)(H_2O)_2]_2[\{Mn(H_2L)(H_2O)\}_2\{Fe(CN)_6\}][\{Mn(H_2L)\}_2\{Fe(CN)_6\}_3].13H_2O$ (19)

The PBP precursor $[Mn(H_2L)Cl(H_2O)]Cl$ undergoes facile self-assembly with $[Fe(CN)_6]^{3-}$ and leads to the formation of a brown insoluble solid. An insoluble amorphous solid was obtained even in the presence of KSCN. However, when the reaction of $[Mn(H_2L)(H_2O)Cl]Cl$ with $K_3[Fe(CN)_6]$ was carried out in presence of

$NaClO_4.H_2O$ at room temperature, two novel cyano bridged complexes, $[\{Mn(H_2L)(H_2O)\}_2\{Mn(H_2L)\}\{Fe(CN)_6\}_2(H_2O)].9H_2O$ (**18**) and $[Mn(H_2L)(H_2O)_2]_2[\{Mn(H_2L)(H_2O)\}_2\{Fe(CN)_6\}][\{Mn(H_2L)\}_2\{Fe(CN)_6\}_3].13H_2O$ (**19**) are obtained as block shaped and needle shaped crystals (Scheme 5.4). The crystals of compounds **18** and **19** were collected separately in good yield.

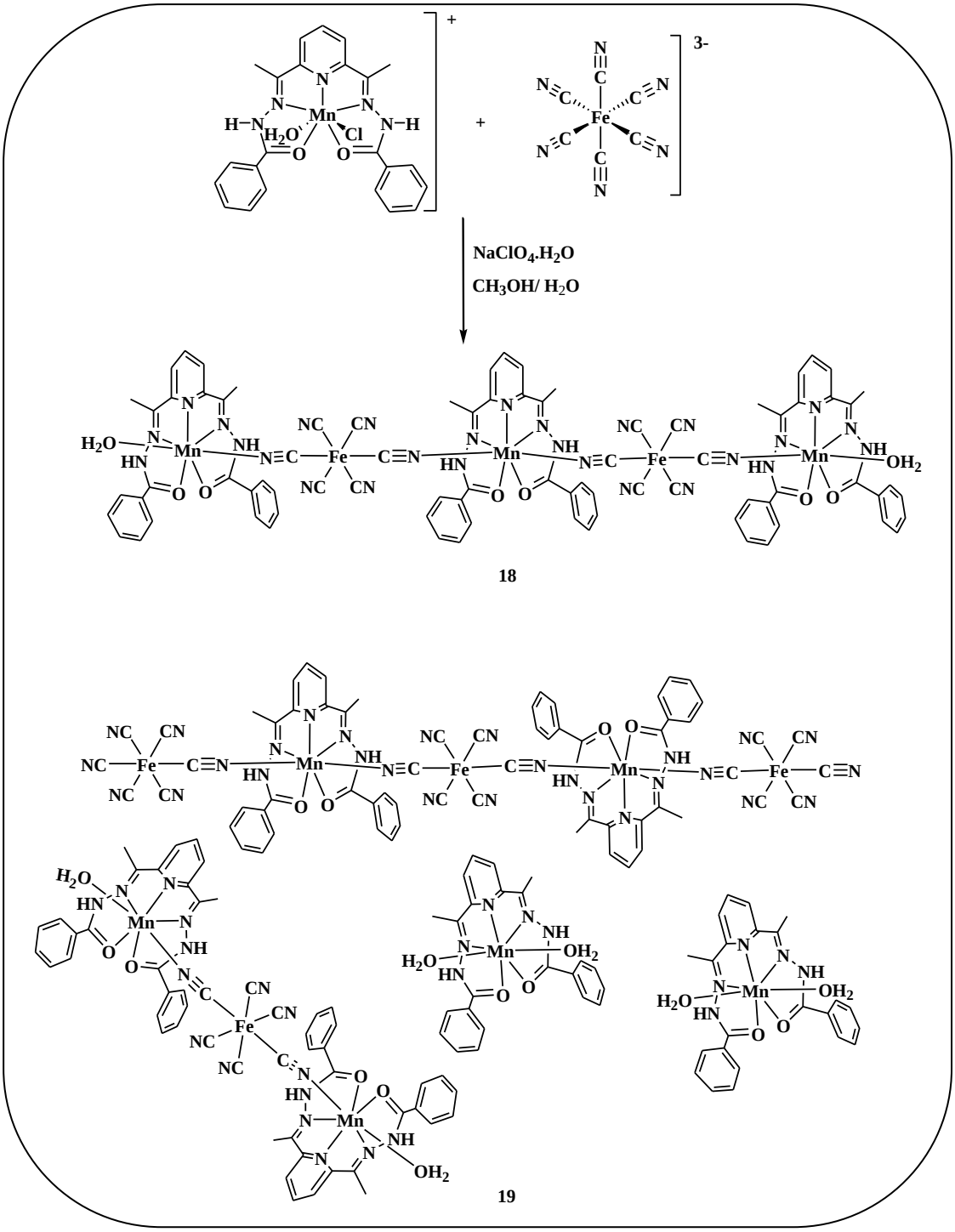

Scheme 5.4. Synthesis of compounds **18** and **19**

The IR spectra of compounds **18** and **19** recorded as KBr discs are depicted in Figure 5.11. The two IR spectra are almost identical apart from slight differences in peak positions. Apart from the characteristic bands of the acyclic ligand, IR spectra of compounds **18** and **19** also show strong absorption peaks at 2116 cm^{-1} and 2115 cm^{-1} respectively. These bands can be easily assigned to -C≡N stretching vibrations of the ferricyanide moiety present in both the complexes. Intense peaks observed at 1622 cm^{-1} and 1625 cm^{-1} for compounds **18** and **19** respectively can be attributed to >C=N stretching vibration of the imine group from the bis-hydrazone ligand, H_2L.

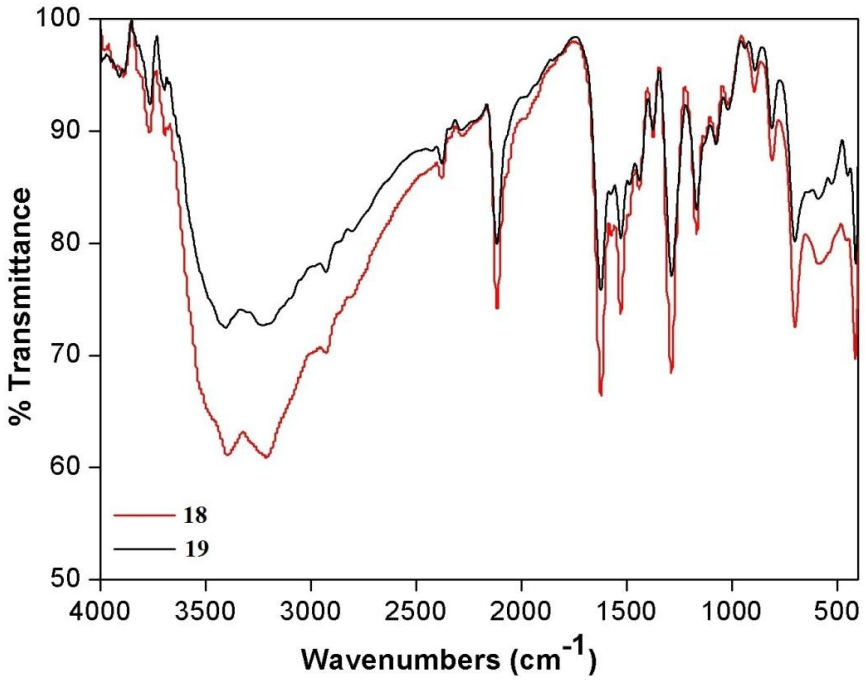

Figure 5.11. FT-IR Spectra of **18** and **19** as KBr diluted discs

5.3.8. Molecular structure of compound 18

Single crystal X-ray structure analysis of compound **18** reveals that it crystallizes in monoclinic C2/c space group. Relevant structural parameters are listed in Table 5.2 while important bond lengths and angles are listed in Table 5.9. It has a linear pentanuclear structure formed by three $[Mn(H_2L)]^{2+}$ and two $[Fe(CN)_6]^{3-}$ moieties. The three $[Mn(H_2L)]^{2+}$ moieties are bridged by two $[Fe(CN)_6]^{3-}$ metalloligands and this leads to the formation of a discrete $[Mn(II)_3Fe(III)_2]$ heterometallic aggregate (Figure 5.12). All three Mn(II) centers in compound **18** retain the PBP geometry and continuous SHAPE analysis of the coordination environment around Mn(II) centers unambiguously suggest a D_{5h} geometry (Table 5.1).

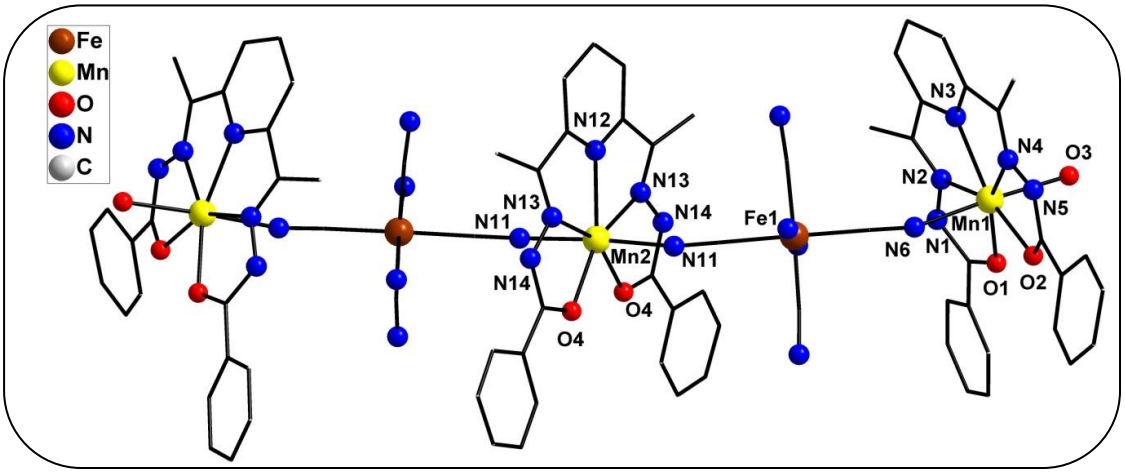

Figure 5.12. Molecular structure of compound **18**. Lattice solvent molecules and hydrogen atoms are omitted for clarity

Both the axial sites of the central Mn(II) are occupied by the nitrogen atoms from cyano groups of ferricyanide anions, while for the terminal Mn(II) centers the axial sites are occupied by an aqua ligand and a nitrogen atom of bridging cyano group from $[Fe(CN)_6]^{3-}$ units. The equatorial coordination sites of all three Mn(II) centers are occupied by donor atoms of the planar pentadentate ligand, H_2L. The cyano groups of $[Fe(CN)_6]^{3-}$ units involved in bridging $[Mn(H_2L)]^{2+}$ are disposed trans to each other. The structural parameters observed for the $[Mn(H_2L)]^{2+}$ units are in good agreement with those observed in case of the mononuclear precursor complex. Moreover, the respective structural parameters observed within the two terminal $[Mn(H_2L)]^{2+}$ units are identical and differ slightly from those observed in case of the central $[Mn(H_2L)]^{2+}$ unit. The terminal Mn-$N_{cyanide}$ distances measure 2.181 Å, while a slightly shorter Mn-$N_{cyanide}$ distance of 2.124 Å is observed for the central Mn(II) center. Both, terminal O-Mn-N and central N-Mn-N linkages are nearly linear as the bond angles are found to be 176.1° and 176.2° respectively. However, all Mn-C-N linkages deviate from linearity as these bond angles are in 155.9-156.4° range. The intramolecular Mn(II)-Fe(III) separation through bridging cyano groups are found to lie within the range of 5.094-5.132 Å and these distances are comparable to those observed in earlier reported Mn(II)-Fe(III) cyano bridged complexes [37-44]. One of the cyano nitrogen atom N(8) is involved in intermolecular H-bonding with hydrogen atom of hydrazone N(2)-H(2A) group from a nearby molecule. This leads to the formation of a H-bonded 1D chain structure as shown in Figure 5.13 and the hydrogen bonding parameters are listed in Table 5.11.

Table 5.9. Selected bond lengths [Å] and angles [°] for compound **18**

Fe(1)-C(41)	1.929(8)	N(6)-Mn(1)-O(1)	93.8(2)
Fe(1)-C(27)	1.936(8)	O(3)-Mn(1)-O(1)	85.4(2)
Fe(1)-C(25)	1.939(8)	N(6)-Mn(1)-N(4)	91.3(2)
Fe(1)-C(24)	1.951(8)	O(3)-Mn(1)-N(4)	87.8(2)
Mn(1)-N(6)	2.181(6)	N(6)-Mn(1)-N(3)	87.5(2)
Mn(1)-O(3)	2.216(6)	O(3)-Mn(1)-N(3)	95.7(2)
Mn(1)-O(1)	2.238(5)	O(1)-Mn(1)-N(3)	135.66(19)
Mn(1)-N(4)	2.280(6)	N(4)-Mn(1)-N(3)	69.0(2)
Mn(1)-N(3)	2.291(6)	N(6)-Mn(1)-O(2)	90.4(2)
Mn(1)-O(2)	2.305(5)	O(3)-Mn(1)-O(2)	85.7(2)
Mn(1)-N(2)	2.340(6)	O(1)-Mn(1)-O(2)	86.14(17)
Mn(2)-N(11)#1	2.124(5)	N(4)-Mn(1)-O(2)	69.3(2)
Mn(2)-N(11)	2.124(5)	N(3)-Mn(1)-O(2)	138.2(2)
Mn(2)-O(4)#1	2.262(6)	O(3)-Mn(1)-N(2)	99.7(2)
Mn(2)-N(13)	2.337(8)	N(6)-Mn(1)-O(1)	93.8(2)
Mn(2)-N(13)#1	2.337(8)	O(3)-Mn(1)-O(1)	85.4(2)
N(12)-C(35)#1	1.324(10)	N(13)-Mn(2)-(13)#1	134.8(4)

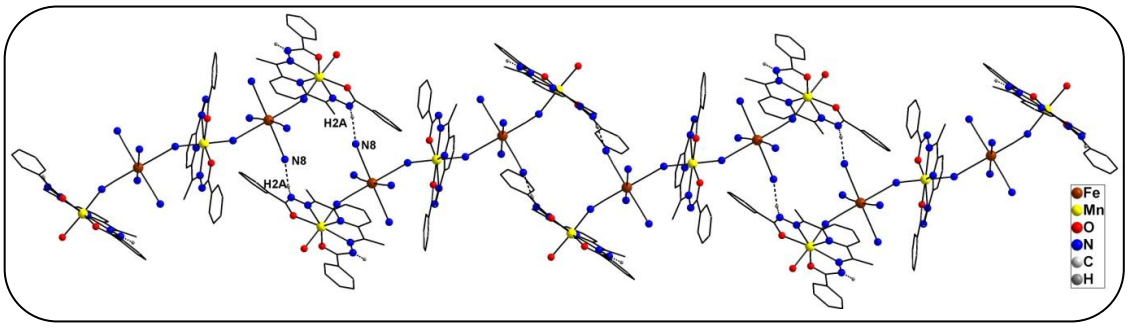

Figure 5.13. Two dimensional hydrogen bonding network present in compound **18**

Table 5.10. Hydrogen bonding parameters of compound **18**

Interactions	**H¨A (Å)**	**D¨A (Å)**	**<D–H...A (◦)**	**Symmetry**
N(1)-H(1A)...O(13)	2.182	3.098(.008)	154.5	½+x, -½+y, z
N(5)-H(2A)...N(8)	2.019	2.851(.010)	171.7	½-x, ½-y, z

5.3.9. Molecular structure of compound 19

Yellow needle shaped crystals of compound **19** crystallizes in P-1 space group. Single crystal X-ray diffraction analysis revealed that compound **19** is a neutral decanuclear species which comprises of isolated pentanuclear, trinuclear and two mononuclear structural motifs within the same molecule (Figure 5.14).

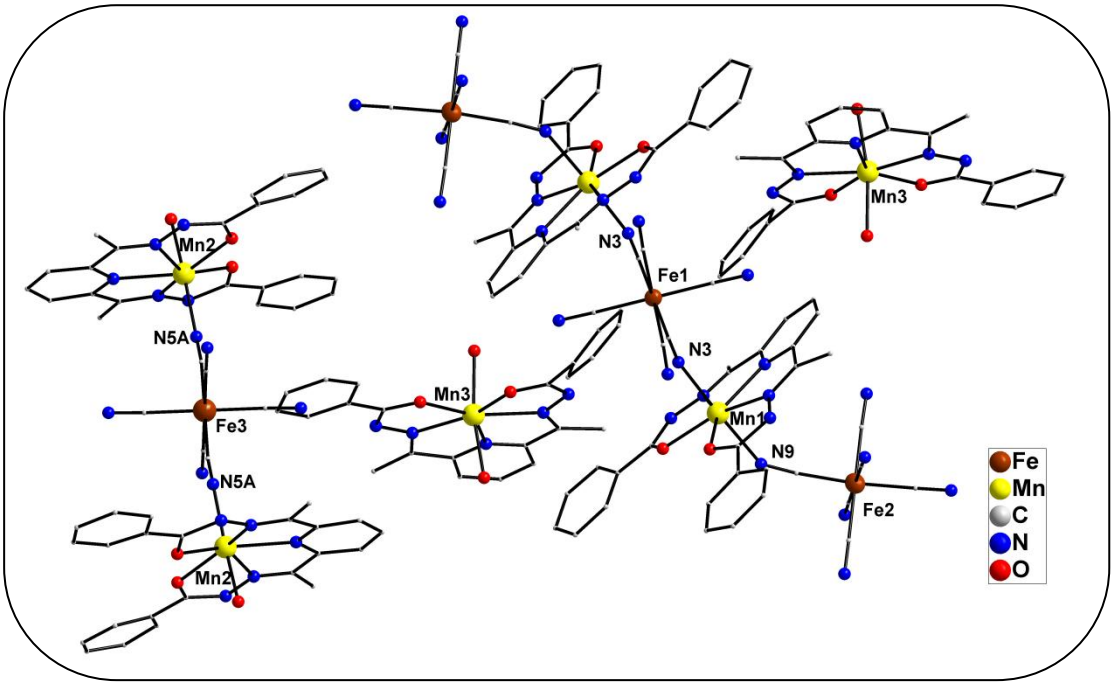

Figure 5.14. Molecular structure of compound **19**. Lattice solvent molecules and hydrogen atoms are omitted for clarity

The pentanuclear, $[Mn(II)_2Fe(III)_3]^{5-}$ motif consist of two $[Mn(H_2L)]^{2+}$ bridged together by three $[Fe(CN)_6]^{3-}$ moieties. Thus, the axial sites of both the $[Mn(H_2L)]^{2+}$ units are occupied by the cyano groups of the neighbouring ferricyanide anions and the Mn(II) centers have slightly distorted PBP geometry with N_5O_2 coordination environment. Meanwhile, the trinuclear, $[Mn(II)_2Fe(III)]^{3+}$ motif consists of two $[Mn(H_2L)]^{2+}$ units bridged by the cyano groups of a $[Fe(CN)_6]$ unit. One of the axial sites of the Mn(II) center is occupied by N atoms of bridging $[Fe(CN)_6]$ group while the other axial site is occupied by O atom of an aquo ligand. Thus, the Mn(II) centers within the trinuclear motifs have distorted PBP geometry with N_5O_2 coordination environment. It is pertinent to note that in compound **19**, the bis-hydrazone ligand of alternate $[Mn(H_2L)]^{2+}$ moieties within the pentanuclear $[Mn(II)_2Fe(III)_3]^{5-}$ motif and trinuclear $[Mn(II)_2Fe(III)]^{3+}$ motif are disposed trans to each other. Apart from the pentanuclear

and trinuclear motifs, two mononuclear $[Mn(H_2L)(H_2O)_2]^{2+}$ units are also present in compound **19** for charge neutrality. The structural parameters observed for all six $[Mn(H_2L)]^{2+}$ moieties within the decanuclear compound **19** are in good agreement with those observed for the precursor complex (Table 5.2). Important bond lengths and bond angles are listed in Table 5.12.

Table 5.11. Selected bond lengths [Å] and bond angles [°] of compound **19**

Fe(1)-C(47)	1.904(10)	C(47)-Fe(1)-C(47)#1	180.0(5)
Fe(1)-C(47)#1	1.904(10)	C(46)#1-Fe(1)-C(48)#1	84.9(3)
Fe(1)-C(46)#1	1.927(9)	N(11)-Mn(2)-O(5)	92.9(2)
Fe(1)-C(48)#1	1.949(9)	N(11)-Mn(2)-N(14)	174.9(3)
Fe(1)-C(48)	1.949(9)	O(5)-Mn(2)-N(14)	90.8(2)
Mn(2)-N(11)	2.219(8)	N(11)-Mn(2)-O(6)	88.7(2)
Mn(2)-O(5)	2.220(6)	O(5)-Mn(2)-O(6)	86.9(2)
Mn(2)-N(14)	2.227(7)	O(6)-Mn(2)-N(9)	68.8(2)
Mn(2)-O(6)	2.303(6)	N(8)-Mn(2)-N(9)	67.5(2)
Mn(2)-N(8)	2.312(7)	N(11)-Mn(2)-N(7)	95.1(2)
Mn(2)-N(9)	2.324(7)	O(5)-Mn(2)-N(7)	68.6(2)
Mn(2)-N(7)	2.330(7)	N(10)-N(9)-Mn(2)	116.9(5)
Mn(1)-O(2)	2.176(6)	O(3)-Mn(1)-N(2)	88.6(2)
Mn(3)-N(22)	2.263(10)	O(15)-Mn(3)-O(8)	87.9(5)
Mn(3)-O(8)	2.269(8)	O(7)-Mn(3)-O(8)	81.1(3)
Mn(3)-N(21)	2.297(11)	N(22)-Mn(3)-O(8)	137.7(4)
Mn(1)-N(2)	2.288(7)	O(15)-Mn(3)-N(21)	80.9(6)

Within the pentanuclear motif in compound **19**, the terminal Mn-$N_{cyanide}$ distances measure 2.227 Å while the inner Mn-$N_{cyanide}$ bond distances measure 2.219 Å. These distances are slightly longer as compared to Mn-$N_{cyanide}$ distances observed in compound **18**. Again for the pentanuclear motif in compound **19**, the N-Mn-N bond angles measuring 174.9° slightly deviate from linearity while the average C-N-Mn bond angle measuring 149.5° significantly deviate from linearity. The intra-motif Mn-Fe separation in the pentanuclear and trinuclear units in compound **19** lie within the

range 5.010-5.198 Å which is comparable to those observed in case of compound **18**. The N atoms of the cyano ligands in the pentanuclear and trinuclear units are interconnected to the oxygen atoms of the mononuclear unit through the intramolecular hydrogen bonds (Table 5.13). A large volume of the crystal lattice is occupied by highly disordered H_2O molecules (approximately 13 H_2O molecules as per PLATON calculated lattice solvent void volume) [59].

Table 5.12. Hydrogen bonding parameters of compound **19**

Interactions	**H···A (Å)**	**D···A (Å)**	**<D–H···A (◦)**	**Symmetry**
N(1)-H(1A)...N(13)	2.092	3.221(0)	173.4	-

5.3.10. Variable temperature magnetic studies

The diamagnetic character of nitroprusside ion in compounds **15-17** impedes magnetic exchange pass-way. Therefore cooperative magnetic phenomena are not expected in these heterometallic assemblies. Nevertheless, magnetization studies on polycrystalline samples of compounds **15** & **17** were performed under a constant static field of 1000 Oe between 2-300 K. Figure 5.15 depicts the variation of $\chi_M T$ with temperature for compound **15**. At 300 K, the $\chi_M T$ product for compound **15** is 4.325 cm^3Kmol^{-1} and that of compound **17** is found to be 4.367 cm^3Kmol^{-1}. This value is close to the expected $\chi_M T$ value of 4.375 cm^3Kmol^{-1} for an isolated high spin Mn(II) center with S =5/2 (considering g=2.0). The $\chi_M T$ product for both compounds **15** & **17** do not change appreciably within the temperature range 10-300 K and this indicates a paramagnetic behaviour. Small increase in $\chi_M T$ product is observed near 50 K and this may be attributed to onset of very weak ferromagnetic interactions mediated by intermolecular H-bonding interactions. Careful analysis of the $\chi_M T$ behaviour of several other nitroprusside based paramagnetic species reported earlier revealed presence of similar weak ferromagnetic couplings [36-44]. On lowering the temperature below 10 K, sharp decrease in $\chi_M T$ is observed for both the complexes. This can be attributed to intermolecular antiferromagnetic coupling mediated through diamagnetic nitroprusside groups.

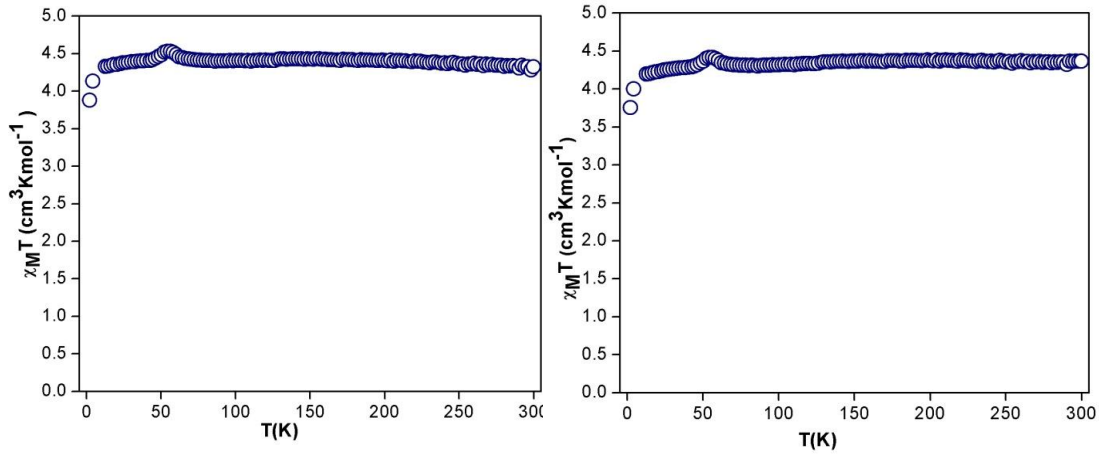

Figure 5.15. Variation of $\chi_M T$ with temperature of compound **15** (left) and **17** (right)

Moreover, the variation of $1/\chi_M$ with temperature reveals an almost linear dependence of $1/\chi_M$ on temperature for both the compounds **15** and **17**. The $1/\chi_M$ behaviour between 5-300K obeys Curie-Weiss law with a Weiss constant θ = -1.59 K and -1.57 K for compounds **15** and **17** respectively. The Curie constant C of compounds **15** and **17** are found to be 4.34 cm^3Kmol^{-1} and 4.27 cm^3Kmol^{-1} respectively. This indicates that both the compounds obey the Curie law for paramagnetic substances (Figure 5.16). The experimental value of C agrees well with the calculated value of 4.37 cm^3Kmol^{-1} for an isolated high spin Mn(II) (S=5/2) and a low spin Fe(III) (S=1/2). Moreover, the sign of Weiss constant indicates the presence of antiferromagnetic interactions between the spin carriers.

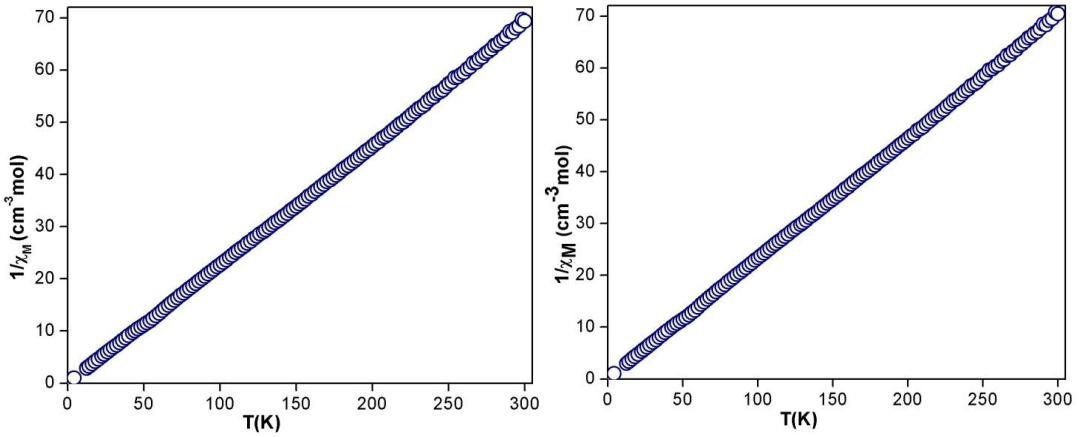

Figure 5.16. Temperature dependence of $1/\chi_M$ of **15** (left) and **17** (right) respectively

The field dependence of magnetization for compounds **15** and **17** at 2 K and 10 K are depicted in Figure 5.17. With increase of field strength, magnetization first increases linearly and at 7 T, magnetization reaches 4.77 and 4.91 Nβ for compounds **15** and **17** respectively. The observed saturation magnetization value is close to the expected

saturation magnetization value of 5.00 Nβ for one Mn(II) center (considering g = 2.00 and S = 5/2).

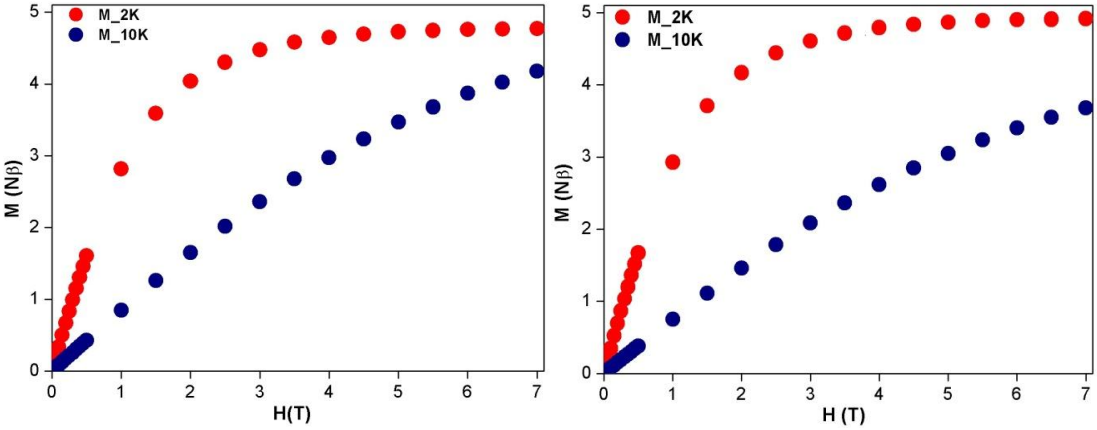

Figure 5.17. Field dependence of magnetization of compound **15** (left) and **17** (right) respectively at 2 K and 10 K

Heterometallic Mn(II)-Fe(III) complexes show interesting magnetic behaviours and therefore such species have been subjected to intense investigation [35-42]. The plot of temperature dependence of $\chi_M T$ for compound **18** is depicted on Figure 5.18. The value of $\chi_M T$ for compound **18** at 300 K is 14.16 cm^3Kmol^{-1} and this agrees well with the expected value of 13.875 cm^3Kmol^{-1} for three isolated high spin Mn(II) and two isolated low spin Fe(III) centers. On lowering the temperature, $\chi_M T$ decreases slowly and reaches 14.08 cm^3Kmol^{-1} at 50 K. On further cooling, $\chi_M T$ decreases sharply to reach a minimum at 35 K (13.83 cm^3Kmol^{-1}) after which an abrupt increase of $\chi_M T$ product upto 16.47 cm^3Kmol^{-1} at 5 K is observed.

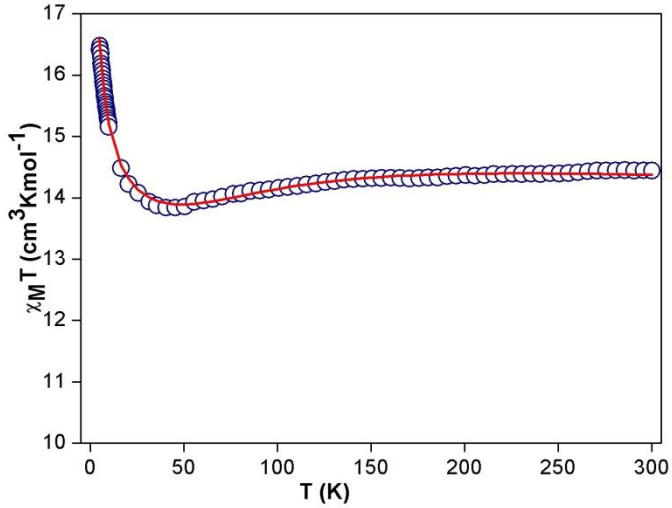

Figure 5.18. Temperature dependence of $\chi_M T$ for compound **18**. Circles represent experimental data and the solid line indicates best fit obtained by using PHI program

The $1/\chi_M$ behaviour between 5-300 K obeys Curie-Weiss law with a Weiss constant θ = -1.85 K and a Curie constant C of 14.088 cm^3Kmol^{-1} (Figure 5.19). The experimental C value is in good agreement with the calculated C value (13.875 cm^3Kmol^{-1}) for three isolated high spin Mn(II) (S = 5/2) and two isolated low spin Fe(III) (S = 1/2) assuming $g_{Mn} = g_{Fe} = 2.0$.

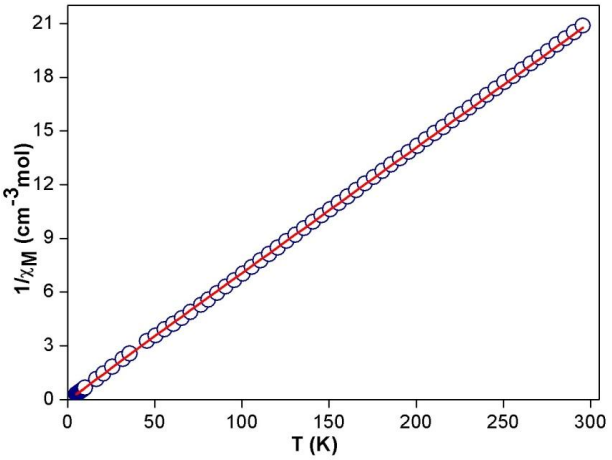

Figure 5.19. Variation of $1/\chi_M$ against temperature for compound **18**. Circles represent experimental value and the solid line represents the best fit obtained by using PHI program

The sign of Weiss constant indicates the presence of antiferromagnetic interactions between the spin carriers in compound **18**. Moreover, both the sign and magnitude of Weiss constant agrees well with the Weiss constants reported for cyano bridged Mn(II)-Fe(III) species. The reduced magnetization plot at 5 K, 7 K and 10 K for compound **18** superimposes on each other (Figure 5.20) which indicates that the compound **18** lacks magnetic anisotropy and accordingly it did not show any out of phase signal during ac susceptibility measurement.

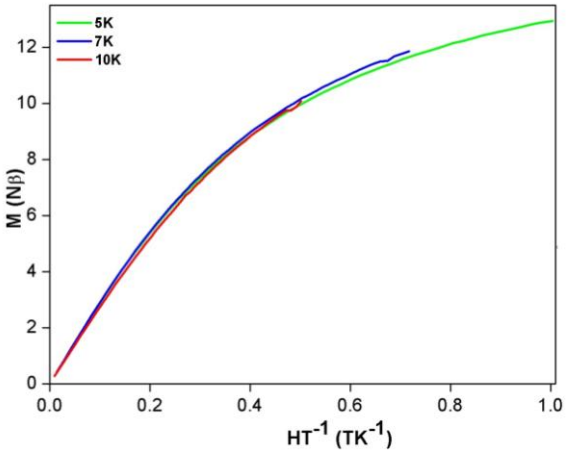

Figure 5.20. Reduced magnetization plot of compound **18**

The field dependence of magnetization of compound **18** at 5 K, 7 K and 10 K is shown in Figure 5.21. With the increase of the applied field strength, the value of magnetization at 5 K increases linearly and reaches upto 12.96 Nβ at 5 K. The calculated value of saturation magnetization for antiferromagnetically coupled pentanuclear unit with three Mn(II) and two Fe(III) centres is 13 Nβ (S_{Mn}=5/2 and S_{Fe}=1/2, assuming g_{Mn}=g_{Fe}=2).

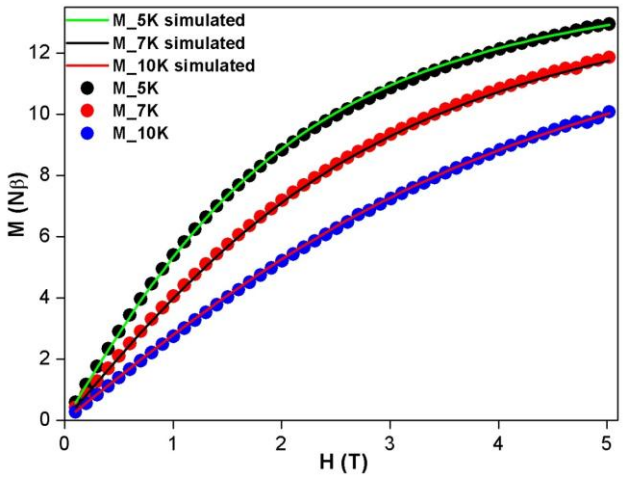

Figure 5.21. Field dependence of magnetization between 0-5 T for compound **18**. Circles represent experimental value and the solid lines are the best fit obtained by using PHI program

The above magnetic behaviour is typical for antiferromagnetically coupled species having irregular spin state structure with a ground spin state of 13/2. Lowering of temperature increases population of the M_s = -13/2 ground state and therefore $\chi_M T$ product increases upto 16.41 cm^3Kmol^{-1} at 5 K. It is pertinent to note here that the calculated $\chi_M T$ product for an isolated S = 13/2 system considering g = 2.0 is 24.375 cm^3Kmol^{-1}. However, due to the weak exchange interaction between the spin carriers the M_s = -13/2 state is not saturated and therefore the observed $\chi_M T$ product remains far below the expected value.

The intramolecular Mn-Fe separations for the terminal and central Mn(II) units in compound **18** are slightly different from each other. Therefore, magnetic coupling between the Mn(II) centers and the adjacent Fe(III) centers are described by two independent coupling constants J_1 (terminal) and J_2 (central) with the following spin Hamiltonian:

$$H = -2J_1(S_{Fe(1)}S_{Mn(1)} + S_{Fe(1A)}S_{Mn(1A)}) - 2J_2S_{Mn(2)}(S_{Fe(1)} + S_{Fe(1A)})$$

Using the above spin Hamiltonian, the $\chi_M T$ data of compound **18** between 5-300 K can be fitted and the best fit parameters are J_1 = -5.59 cm^{-1}, J_2 = -5.64 cm^{-1}, g_{Mn} = 2.07 and g_{Fe} = 2.11. The negative magnetic exchange interactions observed for compound **18** are consistent with earlier reported cyano bridged Mn(II)-Fe(III) complexes.

Magnetization measurements on polycrystalline sample of the decanuclear compound **19** was carried out between 3-300 K and its magnetic properties are found to be quite similar to that of the pentanuclear compound **18**. The experimental $\chi_M T$ value of compound **19** at room temperature is 27.72 cm^3Kmol^{-1}, which slightly deviates from the expected value of 27.75 cm^3Kmol^{-1} for six magnetically non-interacting isolated high Mn(II) centres (S = 5/2) and four isolated low spin Fe(III) centres (S = 1/2) (Figure 5.22).

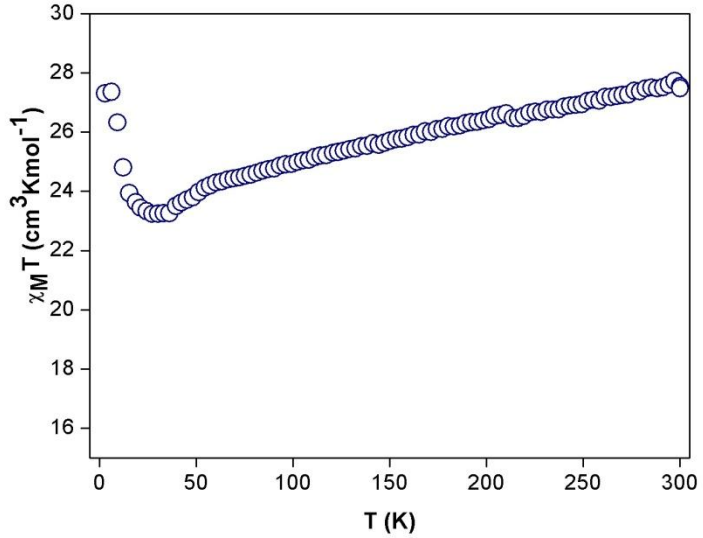

Figure 5.22. Temperature dependence of $\chi_M T$ for compound **19**

On lowering the temperature, the $\chi_M T$ product slightly decreases upto 52 K and then it decreases rapidly to reach a minimum of 23.23 cm^3Kmol^{-1} at 27 K. On further lowering the temperature, the $\chi_M T$ value tends to increase abruptly to 27.30 cm^3Kmol^{-1} at 3K. The $1/\chi_M$ behaviour of compound **19** between 3-300 K conforms well with the Curie-Weiss law and corresponding Weiss constant was θ = -12.39 K while the Curie constant was C = 28.16 cm^3Kmol^{-1} (Figure 5.23). The calculated Curie constant for six isolated high spin Mn(II) and four isolated low spin Fe(III) is 27.75 cm^3Kmol^{-1} and it conforms well with the experimental Curie constant obtained for compound **19**.

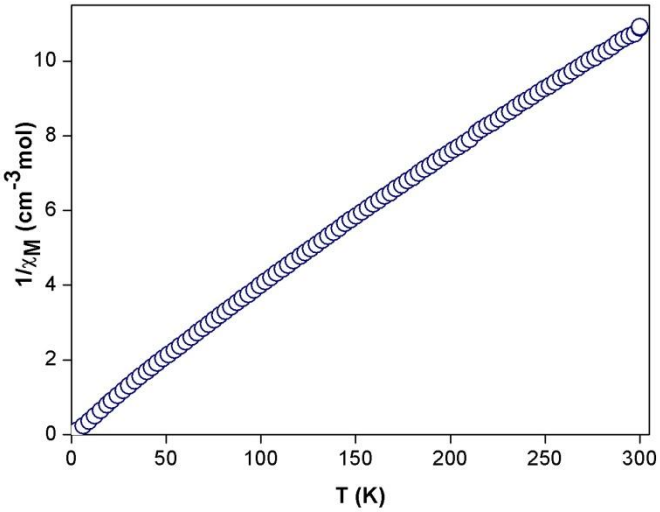

Figure 5.23. Variation of $1/\chi_M$ against temperature for compound **19**.

As in the case of compound **18**, the reduced magnetization plot at 3 K, 5 K, 7 K and 10 K for compound **19** superimposes on each other as depicted in Figure 5.24. This clearly indicates that the compound **19** also lacks magnetic anisotropy and thus it did not show any out of phase signal during ac susceptibility measurement.

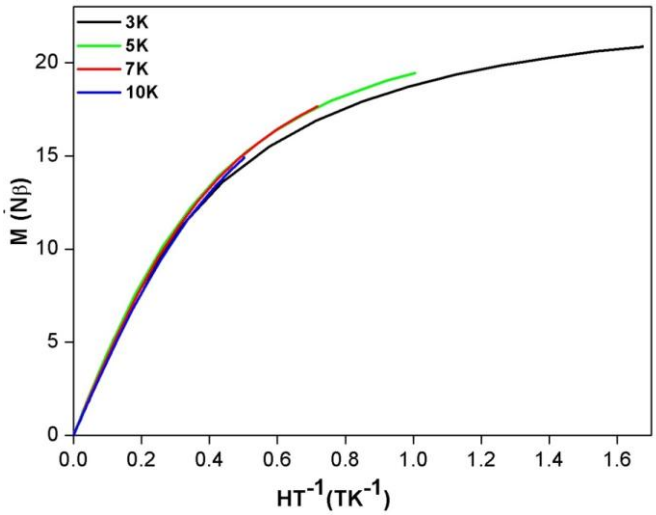

Figure 5.24. Reduced magnetization plot of compound **19**

The field dependence of magnetization of compound **19** at 3 K, 5 K, 7 K and 10 K is shown in Figure 5.25. On increasing the applied field strength, the isothermal magnetization between 3-10 K increases linearly and becomes 20.23 Nβ at 3K under a field of 5 T. The calculated value of saturation magnetization for the decanuclear complex with magnetically non-interacting pentanuclear $[Mn(II)_2Fe(III)_3]$, trinuclear

[$Mn(II)_2Fe(III)$] and two mononuclear Mn(II) units but antiferromagnetic interaction between adjacent spin centers within the same unit is 26 Nβ (S_{Mn}=5/2, S_{Fe}=1/2 and assuming $g_{Mn}=g_{Fe}$=2.0). Thus, compound **19** also has an irregular spin state structure as antiferromagnetic interactions between the spin carriers stabilize an S = 13 spin state at low temperature. Therefore, at low temperature $\chi_M T$ increases abruptly and tends to reach 91 cm^3Kmol^{-1}, the expected $\chi_M T$ for a S = 13 system considering g = 2.0.

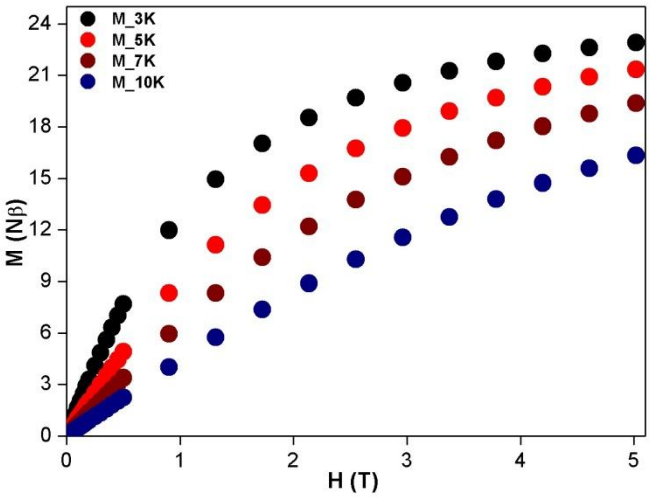

Figure 5.25. Field dependence of magnetization between 0-5 T for compound **19**.

The intramolecular Mn-Fe separations for the terminal and central $[Fe(CN)_6]^{3-}$ units within the pentanuclear motif of compound **19** are not equivalent, as in case of compound **18**. Therefore, magnetic exchange interaction between adjacent spin carriers within the pentanuclear motif of compound **19** are described by two independent coupling constants, J_1(terminal) and J_2(central) with the spin Hamiltonian $H_{penta} = -2J_1(S_{Fe(2)}S_{Mn(2)} + S_{Fe(2A)}S_{Mn(2A)}) -2J_2S_{Fe(1)}(S_{Mn(2)} + S_{Mn(2A)})$. Both the Mn-Fe separations within the trinuclear motif of compound **19** are equivalent and therefore the exchange interaction is described by single coupling constant J_3 with the spin Hamiltonian $H_{Tri} = -2J_3S_{Fe(3)}(S_{Mn(3)} + S_{Mn(3A)})$. Based on these two spin Hamiltonians, the $\chi_M T$ behaviour of compound **19** was fitted using PHI software but due to the large number of metal centres, diagonalization of data was not obtained for compound **19**.

5.4. Conclusions

Thus, the reaction of a PBP Mn(II) precursor, $[Mn(H_2L)(H_2O)Cl]Cl$ with cyanometallate linkers have been investigated and the results obtained are presented in this chapter. It was anticipated that the labile axial ligands present in $[Mn(H_2L)(H_2O)Cl]Cl$ can be easily replaced by cyanometallates and this should lead to the formation of heterometallic cyano bridged architectures. In principle, structures of such heterometallic aggregates should primarily rely on the charge of the precursors. Based on this principle of electroneutrality, a range of structural motifs have been isolated by the reaction of the PBP Mn(II) precursor, $[Mn(H_2L)(H_2O)Cl]Cl$ with the cyanometallate linkers having different charge, e.g. $[Fe(CN)_5(NO)]^{2-}$ and $[Fe(CN)_6]^{3-}$. Moreover, results presented herein show that intricate control over the self assembly process can also be achieved by proper choice of reaction medium. Reaction of $[Mn(H_2L)(H_2O)Cl]Cl$ with $[Fe(CN)_5(NO)]^{3-}$in aqueous methanolic medium immediately leads to the formation of an amorphous solid, which is insoluble in common organic solvents. Presence of an additional anion with coordinating ability can overwhelmingly influence the self-assembly process and results described here suggest that presence of KSCN avert formation of polymeric structure. Therefore, in order to prevent formation of polymeric material, we carried out the reaction of $[Mn(H_2L)(H_2O)Cl]Cl$ with $[Fe(CN)_5(NO)]^{3-}$ in the presence of KSCN. Presence of KSCN prevented the coordination of cyanometallate with the PBP Mn(II) and simple binuclear salt (**15**) of the PBP Mn(II) complex ion with the nitropruisside anion was isolated. Interestingly, it has been observed that presence of excess water in the above reaction impedes isolation of the ionic compound **15** but lead to the crystallization of a neutral bimetallic species **16**. One of the axial sites of the PBP Mn(II) ion is occupied by cyano group of nitroprusside ion and this eventually leads to the formation of the dinuclear heterometallic structure in compound **16**. Moreover, when the reaction leading to the formation of compound **16** was carried out in the absence of KSCN, a 1D polymeric species **17** is formed where both the axial sites of the PBP Mn(II) ion are occupied by cyano groups of nitroprusside ion. The structural motifs **15-17** lack cooperative magnetic properties since the nitroprusside anion is diamagnetic in nature. However, one can anticipate assembling cyanometallate architectures with intriguing magnetic features simply by using paramagnetic cyanometallate precursors. Therefore, reaction of PBP Mn(II) precursor, $[MnL(H_2O)Cl]Cl$ was investigated with a

paramagnetic cyanometalate ion, $[Fe(CN)_6]^{3-}$ and two new cyano bridged Fe(III)-Mn(II) heterometallic aggregates are prepared. The pentanculear structural architecture observed in **18** is quite prevalent, while the structure of decanuclear compound **19** is unique in several aspects. Nevertheless, the relatively large magnetic exchange interaction through the bridging cyano ligand establishes the relevance of cyanometallates in molecular magnetism. Controlled association of cyanometallates in a predetermined fashion will allow us to explore the potential of these species in building molecular magnets with better characteristics.

5.5. References

[1] Gadet, V., Mallah, T., Castro, I., and Verdaguer, M. High-T_c Molecular-Based Magnets: A Ferromagnetic Bimetallic Chromium (III)-Nickel (II) Cyanide with T_c = 90K. *Journal of American Chemical Society*, 114: 9213-9214, 1992.

[2] Miller, J. S. Magnetically ordered molecule-based materials. *Chemical Society Reviews*, 40: 3266-3296, 2011 and references therein.

[3] Dunbar, K. R., Achim, C., and Shatruk, M. *Charge Transfer-Induced Spin-Transitions in Cyanometallate Materials*, John Wiley & Sons, Ltd. 2013.

[4] Beltran, L. M. C. and Long, J. R. Directed Assembly of Metal-Cyanide Cluster Magnets. *Accounts of Chemical Research*, 38(4): 325-334, 2005.

[5] Ohba, M. & Okawa, H. Synthesis and magnetism of multi-dimensional cyanide-bridged bimetallic assemblies. *Coordination Chemical Reviews*, 198(1): 313-328, 2000.

[6] Atanasov, M., Comba, P., Hausberg, S., and Martin, B. Cyanometallate-bridged oligonuclear transition metal complexes-Possibilities for a rational design of SMMs. *Coordination Chemical Reviews*, 253(19-20): 2306-2314, 2009.

[7] Lescouezec, R., Toma, L. M., Vaissermann, J., Verdaguer, M., Delgado, F. S., Ruiz-Pérez, C., Lloret, F., and Julve, M. Design of single chain magnets through cyanide-bearing six-coordinate complexes. *Coordination Chemical Reviews*, 249(23): 2691-2729, 2005.

[8] Sun, H.-L., Wang, Z.-M., and Gao, S. Strategies towards single-chain magnets. *Coordination Chemical Reviews*, 254(9-10): 1081-1100, 2010.

[9] Jeon, I.-R., Calancea, S., Panja, A., Cruz, D. M. P., Koumousi, E. S., Dechambenoit, P., Coulon, C., Wattiaux, A., Rosa, P., Mathonière, C., and

Clérac, R. Spin crossover or intra-molecular electron transfer in a cyanide-bridged Fe/Co dinuclear dumbbell: a matter of state. *Chemical Science*, 4(6): 2463-2470, 2013.

[10] Shatruk, M., Avendano, C., and Dunbar, K. R. Cyanide-Bridged Complexes of Transition Metals: A Molecular Magnetism Prospective. *Progress in Inorganic Chemistry*, 56: 155-334, 2009.

[11] Wang, X.-Y., Avendańo, C., and Dunbar, K. R. Molecular magnetic materials based on 4d and 5d transition metals. *Chemical Society Reviews*, 40(6): 3213-3238, 2011.

[12] Wang, S., Ding, X.-H., Zuo, J.-L., You, X.-Z., and Huang, W. Tricyanometalate molecular chemistry: A type of versatile building blocks for the construction of cyano-bridged molecular architectures. *Coordination Chemistry Reviews*, 255(15-16): 1713-1732, 2011.

[13] Nowicka, B., Korzeniak, T., Stefánczyk, O., Pinkowicz, D., Chorąży, S., Podgajny, R., and Sieklucka, B. The impact of ligands upon topology and functionality of octacyanidometallate-based assemblies. *Coordination Chemical Reviews*, 256(17-18): 1946-1971, 2012 and references therein.

[14] See, for example: Marvaud, V., Decroix, C., Scuiller, A., Guyard-Duhayon, C., Vaissermann, J., Gonnet, F., and Verdaguer, M. Hexacyanometalate molecular chemistry: heptanuclear heterobimetallic complexes; control of the ground spin state. *Chemistry–A European Journal*, 9(8): 1677-1691, 2003.

[15] Marvaud, V., Decroix, C., Scuiller, A., Tuyèras, F., Guyard-Duhayon, C., Vaissermann, J., and Verdaguer, M. Hexacyanometalate Molecular Chemistry: Di-, Tri-, Tetra-, Hexa-and Heptanuclear Heterobimetallic Complexes; Control of Nuclearity and Structural Anisotropy. *Chemistry-A European Journal*, 9(8): 1692-1705, 2003.

[16] Parker, R. J., Spiccia, L., Batten, S. R., Cashion, J. D., and Fallon, G. D. The encapsulation of ferrocyanide by copper (II) complexes of tripodal tetradentate ligands. Novel H-bonding networks incorporating heptanuclear and pentanuclear heterometallic assemblies. *Inorganic Chemistry*, 40(18): 4696-4704, 2011.

[17] Parker, R. J., Spiccia, L., Moubaraki, B., Murray, K. S., Hockless, D. C., Rae, A. D., and Willis, A. C. Structure and magnetism of heptanuclear complexes formed

on encapsulation of hexacyanoferrate (II) with the Mn (II) and Ni (II) complexes of 1, 4-bis (2-pyridylmethyl)-1, 4, 7-triazacyclononane. *Inorganic Chemistry*, 41(9): 2489-2495, 2002.

[18] Ferlay, S., Mallah, T., Vaissermann, J., Bartolomé, F., Veillet, P., and Verdaguer, M. A chromium (III) nickel (II) cyanide-bridged ferromagnetic layered structure with corrugated sheets. *Chemical Communications*, 21: 2481-2482, 1996.

[19] Colacio, E., Domínguez-Vera, J. M., Ghazi, M., Moreno, J. M., Kivekäs, R., Lloret, F., and Stoeckli-Evans, H. A novel two-dimensional honeycomb-like bimetallic iron (III)–nickel (II) cyanide-bridged magnetic material $[Ni(cyclam)]_3[Fe(CN)_6]_2 \cdot nH_2O$ (cyclam = 1, 4, 8, 11-tetraazacyclodecane). *Chemical Communications*, 11: 987-988, 1999.

[20] Marvilliers, A., Parsons, S., Rivière, E., Audière, J. P., Kurmoo, M., and Mallah, T. Structure, Magnetic Properties and Magnetic Phase Diagram of a Layered, Bimetallic, Cyanide-Bridged Cr^{III}-Ni^{II} Metamagnet. *European Journal of Inorganic Chemistry*, 2001(5): 1287-1293, 2001.

[21] Kou, H. Z., Gao, S., Ma, B. Q., and Liao, D. Z. A cyano-bridged molecular magnet with a novel two-dimensional brick wall structure. *Chemical Communications*, 14: 1309-1310, 2000.

[22] Ni, Z. H., Kou, H. Z., Zhang, L. F., Ni, W. W., Jiang, Y. B., Cui, A. L., and Sato, O. mer-$[Fe(pcq)(CN)_3]^-$: A Novel Cyanide-Containing Building Block and Its Application to Assembling Cyanide-Bridged Trinuclear $Fe^{III}_2Mn^{II}$ Complexes [pcq = 8-(Pyridine-2-carboxamido) quinoline Anion]. *Inorganic Chemistry*, 44(26): 9631-9633, 2005.

[23] Ni, Z. H., Kou, H. Z., Zheng, L., Zhao, Y. H., Zhang, L. F., Wang, R. J., and Sato, O. Assembly of azido-or cyano-bridged binuclear complexes containing the bulky $[Mn(phen)_2]^{2+}$ building block: syntheses, crystal structures, and magnetic properties. *Inorganic Chemistry*, 44(13): 4728-4736, 2005.

[24] Ni, Z. H., Kou, H. Z., Zhao, Y. H., Zheng, L., Wang, R. J., Cui, A. L., and Sato, O. $[Fe(bpb)(CN)_2]^-$ as a Versatile Building Block for the Design of Novel Low-Dimensional Heterobimetallic Systems: Synthesis, Crystal Structures, and Magnetic Properties of Cyano-Bridged Fe^{III}-Ni^{II} Complexes $[(bpb)^{2-}$= 1, 2-Bis

(pyridine-2-carboxamido) benzenate]. *Inorganic Chemistry*, 44(6): 2050-2059, 2005.

[25] Ni, Z. H., Zhang, L. F., Tangoulis, V., Wernsdorfer, W., Cui, A. L., Sato, O., and Kou, H. Z. Substituent effect on formation of heterometallic molecular wheels: Synthesis, crystal structure, and magnetic properties. *Inorganic Chemistry*, 46(15): 6029-6037, 2007.

[26] Venkatakrishnan, T. S., Sahoo, S., Bréfuel, N., Duhayon, C., Paulsen, C., Barra, A. L., and Sutter, J. P. Enhanced ion anisotropy by nonconventional coordination geometry: single-chain magnet behavior for a $[\{Fe^{II}L\}_2\{Nb^{IV}(CN)_8\}]$ helical chain compound designed with heptacoordinate Fe^{II}. *Journal of the American Chemical Society*, 132(17): 6047-6056, 2010.

[27] Ruamps, R., Batchelor, L. J., Maurice, R., Gogoi, N., Jiménez-Lozano, P., Guihéry, N., and Mallah, T. Origin of the Magnetic Anisotropy in Heptacoordinate Ni^{II} and Co^{II} Complexes. *Chemistry-A European Journal*, 19(3): 950-956, 2013.

[28] Huang, X. C., Zhou, C., Shao, D., and Wang, X. Y. Field-Induced Slow Magnetic Relaxation in Cobalt (II) Compounds with Pentagonal Bipyramid Geometry. *Inorganic Chemistry*, 53(24): 12671-12673, 2014.

[29] Dey, M., Dutta, S., Sarma, B., Deka, R. C., and Gogoi, N. Modulation of the coordination environment: a convenient approach to tailor magnetic anisotropy in seven coordinate Co(II) complexes. *Chemical Communications*, 52(4): 753-756, 2016.

[30] Antal, P., Drahoš, B., Herchel, R., and Trávníček, Z. Late First-Row Transition-Metal Complexes Containing a 2-Pyridylmethyl Pendant-Armed 15-Membered Macrocyclic Ligand. Field-Induced Slow Magnetic Relaxation in a Seven-Coordinate Cobalt (II) Compound. *Inorganic Chemistry*, 55(12): 5957-5972, 2016.

[31] Batchelor, L. J., Sangalli, M., Guillot, R., Guihéry, N., Maurice, R., Tuna, F., and Mallah, T. Pentanuclear cyanide-bridged complexes based on highly anisotropic Co^{II} seven-coordinate building blocks: synthesis, structure, and magnetic behavior. *Inorganic Chemistry*, 50(23): 12045-12052, 2011.

[32] Bar, A. K., Pichon, C., Gogoi, N., Duhayon, C., Ramasesha, S., and Sutter, J. P. Single-ion magnet behaviour of heptacoordinated Fe(II) complexes: on the importance of supramolecular organization. *Chemical Communications*, 51(17): 3616-3619, 2015.

[33] Gogoi, N., Thlijeni, M., Duhayon, C., and Sutter, J. P. Heptacoordinated Nickel(II) as an Ising-Type Anisotropic Building Unit: Illustration with a Pentanuclear $[(NiL)_3\{W(CN)_8\}_2]$ Complex. *Inorganic Chemistry*, 52(5): 2283-2285, 2013.

[34] Shao, D., Shi, L., Zhang, S. L., Zhao, X. H., Wu, D. Q., Wei, X. Q., and Wang, X. Y. Syntheses, structures, and magnetic properties of three new chain compounds based on a pentagonal bipyramidal Co(II) building block. *CrystEngComm*, 18(22): 4150-4157, 2016.

[35] Kaur Sra, A., Andruh, M., Kahn, O., Golhen, S., Ouahab, L., and Yakhmi, J. V. A Mixed-Valence and Mixed-Spin Molecular Magnetic Material:$[Mn^{II}L]_6[Mo^{III}(CN)_7][Mo^{IV}(CN)_8]_2\cdot 19.5H_2O$. *Angewandte Chemie International Edition*, 38(17): 2606-2609, 1999.

[36] Tanase, S., Andruh, M., Stanica, N., Mathonière, C., Rombaut, G., Golhen, S., and Ouahab, L. A novel cyano-bridged pentanuclear complex:$[\{Mn_3(MAC)_3(H_2O)_2\}\{Fe(CN)_6\}_2]\cdot 6H_2O\cdot 2CH_3OH$-synthesis, crystal structure and magnetic properties (MAC = pentaaza macrocyclic ligand). *Polyhedron*, 22(10): 1315-1320, 2003.

[37] Bonadio, F., Senna, M. C., Ensling, J., Sieber, A., Neels, A., Stoeckli-Evans, H., and Decurtins, S. Cyano-Bridged Structures Based on $[Mn^{II}(N_3O_2$-Macrocycle$)]^{2+}$: A Synthetic, Structural, and Magnetic Study. *Inorganic Chemistry*, 44(4): 969-978, 2005.

[38] Paraschiv, C., Andruh, M., Journaux, Y., Žak, Z., Kyritsakas, N., and Ricard, L. Trinuclear magnetic clusters based on cyanide metal complexes: synthesis, crystal structures, and magnetic properties of four new $[Mn^{II}_2M^{III}]$ complexes (M= Cr, Fe, Co). *Journal of Materials Chemistry*, 16(26): 2660-2668, 2006.

[39] Zhang, D., Wang, H., Chen, Y., Ni, Z. H., Tian, L., and Jiang, J. Rational Design and Assembly of a New Series of Cyanide-Bridged Fe^{III}-Mn^{II} One-Dimensional

Single Chain Complexes: Synthesis, Crystal Structures, and Magnetic Properties. *Inorganic Chemistry*, 48(12): 5488-5496, 2009.

[40] Wang, X. Y., Prosvirin, A. V., and Dunbar, K. R. A docosanuclear $\{Mo_8Mn_{14}\}$ cluster based on $[Mo(CN)_7]^{4-}$. *Angewandte Chemie International Edition*, 49(30): 5081-5084, 2010.

[41] Wang, Q. L., Southerland, H., Li, J. R., Prosvirin, A. V., Zhao, H., and Dunbar, K. R. Crystal-to-Crystal Transformation of Magnets Based on Heptacyanomolybdate (III) Involving Dramatic Changes in Coordination Mode and Ordering Temperature. *Angewandte Chemie International Edition*, 51(37): 9321-9324, 2012.

[42] Dey, M., Sarma, B., and Gogoi, N. Coligand Promoted Controlled Assembly of Hierarchical Heterobimetallic Nitroprusside Based Aggregates. *Zeitschrift für Anorganische und Allgemeine Chemie*, 640(14): 2962-2967, 2014.

[43] Huang, X. C., Zhou, C., Shao, D., and Wang, X. Y. Field-Induced Slow Magnetic Relaxation in Cobalt (II) Compounds with Pentagonal Bipyramid Geometry. *Inorganic Chemistry*, 53(24): 12671-12673, 2014.

[44] Giordano, T. J., Palenik, G. J., Palenik, R. C., and Sullivan, D. A. Pentagonal-bipyramidal complexes. Synthesis and characterization of aqua (nitrato)[2,6-diacetylpyridine bis (benzoyl hydrazone)] cobalt (II) nitrate and diaqua [2, 6-diacetylpyridine bis (benzoyl hydrazone)] nickel (II) nitrate dihydrate. *Inorganic Chemistry*, 18(9): 2445-2450, 1979.

[45] Lorenzini, C., Pelizzi, C., Pelizzi, G., & Predieri, G. Investigation into aroylhydrazones as chelating agents. Part 3. Synthesis and spectroscopic characterization of complexes of Mn^{II}, Co^{II}, Ni^{II}, Cu^{II}, and Zn^{II} with 2,6-diacetylpyridine bis (benzoylhydrazone) and X-ray structure of aquachloro [2,6-diacetylpyridine bis (benzoylhydrazone)] manganese (II) chloride. *Journal of the Chemical Society, Dalton Transactions*, (4), 721-727, 1983.

[46] Batchelor, L. J., Sangalli, M., Guillot, R., Guihéry, N., Maurice, R., Tuna, F., and Mallah, T. Pentanuclear cyanide-bridged complexes based on highly anisotropic Co^{II} seven-coordinate building blocks: synthesis, structure, and magnetic behavior. *Inorganic Chemistry*, 50(23): 12045-12052, 2011.

[47] Gütlich, P., Garcia, Y., and Woike, T. Photoswitchable coordination compounds. *Coordination Chemistry Reviews*, 219: 839-879, 2001.

[48] Coppens, P., Novozhilova, I., and Kovalevsky, A. Photoinduced linkage isomers of transition-metal nitrosyl compounds and related complexes. *Chemical Reviews*, 102(4): 861-884, 2002 and references therein.

[49] Sheldrick, G. M. A short history of SHELX. *Acta Crystallographica Section A: Foundations of Crystallography*, 64(1): 112-122, 2008.

[50] Llunell, M., Casanova, D., Cirera, J., Bofill, J. M., Alemany, P., Alvarez, S., Pinsky, M. and Avnir, D. *SHAPE: Continuous shape measures of polygonal and polyhedral molecular fragments*; University of Barcelona: Barcelona, 2005.

[51] Ni, W. W., Kou, H. Z., Ni, Z. H., and Wang, R. J. Synthesis, crystal structures, and properties of two manganese (II)-nitroprusside complexes. *Journal of Chemical Crystallography*, 36(1): 47-54, 2006.

[52] Clemente-Leon, M., Coronado, E., Galan-Mascaros, J. R., Gomez-Garcia, C. J., Woike, T., and Clemente-Juan, J. M. Bimetallic Cyanide-Bridged Complexes Based on the Photochromic Nitroprusside Anion and Paramagnetic Metal Complexes. Syntheses, Structures, and Physical Characterization of the Coordination Compounds $[Ni(en)_2]_4[Fe(CN)_5NO]_2[Fe(CN)_6]\odot 5H_2O$, $[Ni(en)_2][Fe(CN)_5NO]\odot 3H_2O$, $[Mn(3\text{-}MeOsalen)(H_2O)]_2[Fe(CN)_5NO]$ and $[Mn(5\text{-}Brsalen)]_2[Fe(CN)_5NO]$. *Inorganic Chemistry*, 40(1): 87-94, 2001.

[53] Shaikh, N., Panja, A., Goswami, S., Banerjee, P., Kubiak, M., Ciunik, Z., and Legendziewicz, J. Synthesis, crystal structure and magnetic properties of cyanide bridged 2D coordination polymers $[Mn\ (salen)]_2[Fe(CN)_5NO]$ and $[Mn(salen)]_2[Ni(CN)_4]$. *Indian Journal of Chemistry Section A*, 43: 1403-1408, 2004.

[54] Peresypkina, E. V., and Vostrikova, K. E. $2[Mn(acacen)]^+ + 1[Fe(CN)_5NO]^-$ polynuclear heterobimetallic coordination compounds of different dimensionality in the solid state. *Dalton Transactions*, 41(14): 4100-4106, 2012.

[55] Ababei, R., Li, Y. G., Roubeau, O., Kalisz, M., Brefuel, N., Coulon, C., and Clerac, R. Bimetallic cyanido-bridged magnetic materials derived from manganese (III) Schiff-base complexes and pentacyanidonitrosylferrate (II) precursor. *New Journal of Chemistry*, 33(6): 1237-1248, 2009.

[56] Yang, C., Wang, Q. L., Ma, Y., Tang, G. T., Liao, D. Z., Yan, S. P., and Cheng, P. Bimetallic Materials Derived from Manganese (III) Schiff Base Complexes and Pentacyanidonitrosylferrate (II) Precursor: Structures and Magnetic Properties. *Inorganic Chemistry*, 49(5): 2047-2056, 2010.

[57] Shu, H. Q., Xu, Y., and Shen, X. P. Synthesis, Crystal Structure and Magnetic Property of a Cyano-Bridged Two-Dimensional Heterometallic Assembly $[Mn(salen)]_2[Fe(CN)_5NO].2H_2O$. *Journal of Chemical Crystallography*, 41(8): 1218-1223, 2011.

[58] Liang, S. W., Li, M. X., Shao, M., and& Liu, H. J. Cyano-bridged bimetallic complexes based on nitroprusside $[Fe(CN)_5(NO)]^{2-}$ and [Cu(TAAB-macrocycle)]$^{2+}$: Synthesis, structure and thermal stability. *Journal of Molecular Structure*, 841(1): 73-77, 2007.

[59] Spek, A. L. PLATON; The University of Utrecht: Utrecht, *The Netherlands*, 1999.